Memorandum

ITASCA
Consulting Group, Inc.

Date: April 5, 2019

To: PFC 6 Documentation Set

From: David Potyondy

Re: Material-Modeling Support for *PFC* [fistPkg6.5]

Ref: ICG7766-L

This memo describes material-modeling support for *PFC* 6.0 as provided in the PFC 6.0 FISHTank (or **`fistPkg`**), and this memo corresponds with **`fistPkg6.5`**.

The following capabilities are provided by **`fistPkg6.5`**:

- Material genesis of linear, contact-bonded, parallel-bonded, flat-jointed and user-defined (3D hill) materials in polyaxial, cylindrical and spherical physical vessels or polyaxial periodic vessel. Material grains can be either balls or clumps. Stress can be installed into the finalized periodic ensemble (after bonding), and then this ensemble can be converted into a periodic brick which is assembled into a larger geometric shape. Material tests are compression (confined, unconfined and uniaxial strain), diametral-compression and direct-tension. Microstructural monitoring includes properties (such as grain-size distribution) with microstructural plot sets and crack monitoring for bonded materials.

Usage instructions are given in **`fistPkg-README.txt`** and summarized as:

- Create a 2D or 3D material (using the appropriate **`MatGen`** project).
- Perform compression, diametral-compression and direct-tension tests on the material (using the **`CompTest`**, **`DiamCompTest`** and **`TenTest`** projects).

111 Third Avenue South • Suite 450 • Minneapolis, Minnesota 55401
Tel: (612) 371-4711 • icg@itascacg.com • www.itascacg.com • Fax: (612) 371-4717

TABLE OF CONTENTS

The PFC model provides a synthetic material consisting of an assembly of rigid grains that interact at contacts.[1] This synthetic material encompasses a vast microstructural space, and only a small portion of this space has been explored. For example, the bonded-particle modeling methodology provides a rich variety of microstructural models in the form of bonded materials (Potyondy, 2015; Potyondy and Cundall, 2004).[2] The PFC model includes both granular and bonded materials as well as an interface that can be inserted into the bonded materials. The support for material modeling that is provided by *PFC2D* and *PFC3D* version 6.0 is described in this document. The material-modeling support is provided in the form of a consistent set of FISH functions, which we call the *PFC FISHTank* (or **`fistPkg`**).[3] The PFC FISHTank provides a state of the art embodiment of four well-defined materials and a user-defined material to support: practical applications (via boundary-value models made from these materials), and scientific inquiry (via further exploration of the microstructural space described above).

The PFC model is described in Section 1.0. The synthetic materials and interface are described in Section 2.0. The microstructural monitoring support is described in Section 3.0. The material-genesis procedure that creates the material is described in Section 0. The testing procedures that perform standard rock-mechanics laboratory tests upon the material are described in Section 5.0. The tests are used to measure mechanical properties and observe microstructural behavior. The properties and behaviors are typically compared with that of the physical material. A stress-installation procedure that initializes stress in the material for subsequent use in boundary-value modeling is described in Section 6.0. Examples of each synthetic material are provided in the three extensions of this memo, which are named "Material-Modeling Support for *PFC* (Example Materials 1, 2 and 3)."

[1] Particles in the PFC model interact at contacts by means of a generalized internal force. Contact mechanics is embodied in particle-interaction laws that employ a soft-contact approach for which all deformation occurs at the contacts between the rigid bodies. The particle-interaction laws are referred to as contact models. The PFC contact models are described in Itasca (2018, PFC: PFC Model Objects: Contacts and Contact Models).

[2] A bonded material is defined as a packed assembly of rigid grains joined by deformable and breakable cement at grain-grain contacts to which larger-scale joints can be added and whose mechanical behavior is simulated by the distinct-element method using the two- and three-dimensional programs *PFC2D* and *PFC3D*.

[3] The material-modeling support package can be downloaded from the link: https://www.itascacg.com/material-modeling-support. The package for PFC 5.0 uses the naming convention **`fistPkgM`**, where **`M`** is the package version number. The package for PFC 6.0 using the naming convention **`fistPkg6.N`**, where **`N`** is the package version number. Material-modeling support may be provided in future versions of *PFC* by embedding the material-modeling capability directly into the command set of the PFC programs.

1.0 PFC MODEL

The PFC programs (*PFC2D* and *PFC3D*) provide a general purpose, distinct-element modeling framework that includes a computational engine and a graphical user interface. A particular instance of the distinct-element model is referred to as a *PFC model*, which refers to both the 2D and 3D models. The PFC model simulates the movement and interaction of many finite-sized particles.[4] The particles are rigid bodies with finite mass that move independently of one another and can both translate and rotate. Particles interact at pair-wise contacts by means of an internal force and moment. Contact mechanics is embodied in particle-interaction laws that update the internal forces and moments. The time evolution of this system is computed via the distinct-element method, which provides an explicit dynamic solution to Newton's laws of motion. The PFC model provides a synthetic material consisting of an assembly of rigid grains that interact at contacts and includes both granular and bonded materials.

We here generalize and expand upon the definition of the PFC model given above — refer to Potyondy (2015) and Itasca (2018) for a comprehensive definition of the PFC model. Potyondy (2015) summarizes the development of the bonded-particle modeling methodology, generalizes our view of the BPM to consist of a base material (of rigid grains joined by deformable and breakable cement at grain-grain contacts) to which larger-scale joints can be added, describes and classifies the rich variety of microstructural models that can be produced, discusses current limitations and suggests avenues for further development.

The PFC model simulates the movement of particles and their mechanical interaction at pair-wise contacts. We denote each particle as a *body* to clarify that it is not a point mass, but instead, is a rigid body with finite mass and a well-defined surface. The PFC model consists of bodies and *contacts* (see Figure 1). There are three types of bodies: *balls*, *clumps* and *walls*. Bodies have surface properties that are assigned to the *pieces* on the body surface. A ball consists of one piece, which is the ball itself, while the pieces of a clump and wall are called *pebbles* and *facets*, respectively. A ball is a rigid unit-thickness disk in 2D or sphere in 3D. A clump is a collection of pebbles that are rigid unit-thickness disks in 2D or spheres in 3D. The 2D model consists of unit-thickness disks (see Figure 2). Clumps model arbitrarily shaped rigid bodies. The pebbles comprising a clump can overlap but contacts do not exist between them; instead, contacts form between the pebbles on the boundary of a clump and other bodies. A wall is a collection of facets that are linear segments in 2D or triangles in 3D and that form a manifold and orientable surface.

Contact mechanics is embodied in particle-interaction laws that employ a soft-contact approach for which all deformation occurs at the contacts between the rigid bodies. The mechanical interaction

[4] The thermal capability expands our definition of the PFC model to include the simulation of transient heat conduction and storage as well as the development of thermally induced displacements and forces. The expanded PFC model simulates the movement and both mechanical and thermal interaction of many finite-sized particles. This document describes the simpler PFC model for which all interactions are mechanical and occur at mechanical contacts.

between the surfaces of two bodies occurs at one or more pair-wise mechanical contacts. Contacts are created and deleted based on body proximity by the contact-detection logic. A contact provides an interface between two pieces.[5] The interface consists of a contact plane with location $(\mathbf{x}_c)$, normal direction $(\hat{\mathbf{n}}_c)$ and coordinate system (nst). The contact plane is centered within the interaction volume (either gap or overlap) of the two pieces, oriented tangential to the two pieces and rotated to ensure that relative motion of the piece surfaces remains symmetric w.r.t. the contact plane. Each contact stores a force $(\mathbf{F}_c)$ and moment $(\mathbf{M}_c)$ that act at the contact location in an equal and opposite sense on the two pieces.[6] The internal force and moment are updated by the particle-interaction law, which takes the relative motion and surface properties of the two pieces as input. We refer to the particle-interaction law as a *contact model.*

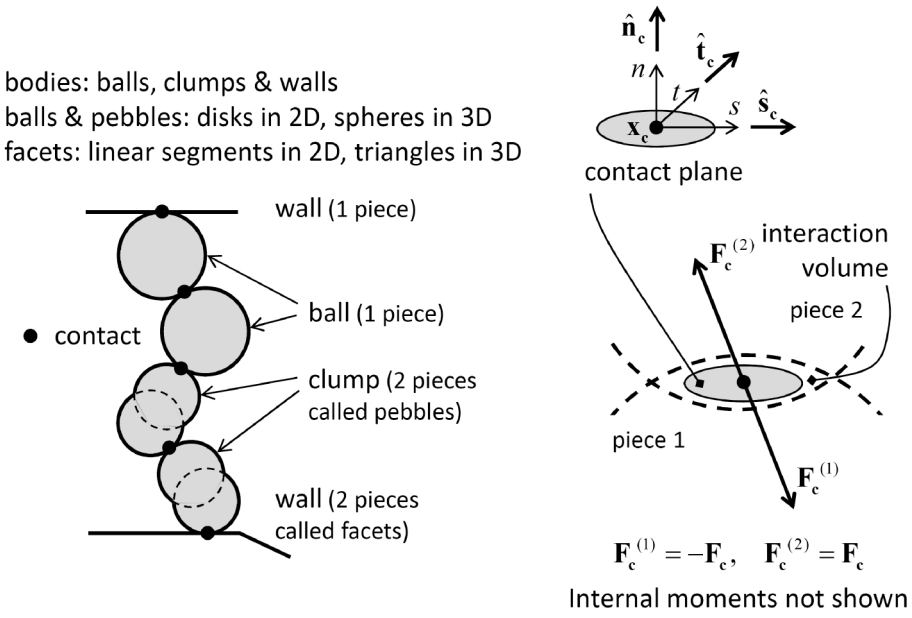

Figure 1 ***PFC model showing bodies and contacts (left) and contact plane with internal force (right).*** (From Fig. 1 of Itasca [2018][7].)

[5] Contacts are referred to by the types of the two pieces. For example, a contact between a ball and facet is called a ball-facet contact and has a contact type of ball-facet. In the current PFC model, facet-facet contacts are not allowed and piece 1 is a ball or pebble while piece 2 is a ball, pebble or facet to give six contact types: ball-ball, ball-pebble, ball-facet, pebble-ball, pebble-pebble and pebble-facet. For most purposes, we do not differentiate between ball-pebble and pebble-ball contacts so that there are five contact types.

[6] Contact models that simulate interaction at a distance update the force and two moments that need not be equal and opposite.

[7] In documentation set at PFC: PFC Model Formulation: Model Components.

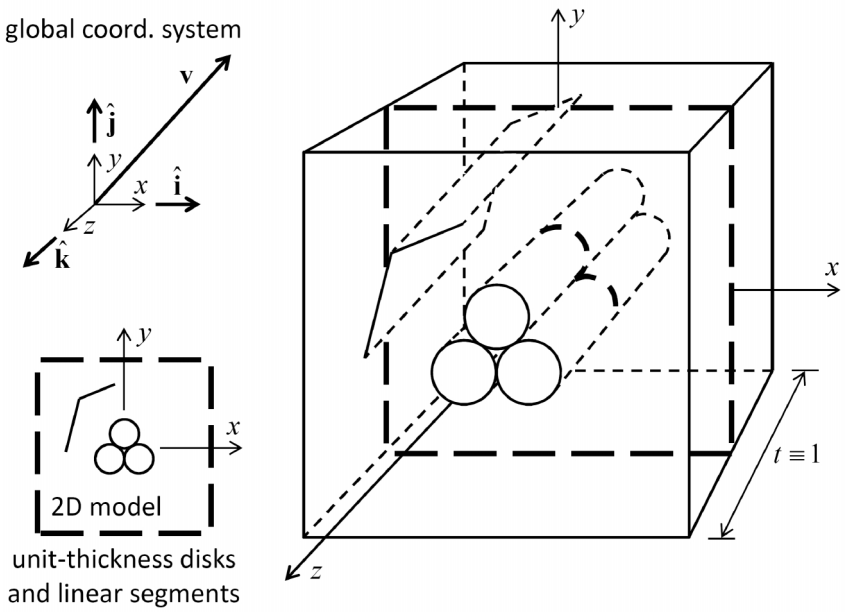

Figure 2 Global coordinate system and orientation of the 2D model, which consists of unit-thickness disks and linear segments centered in the xy plane.

The modeling philosophy that underlies both the development and application of the PFC model (and which includes the importance of having a well-defined model of a system, and the limitations of any such model) is well stated in the following excerpt from the chapter "Models and Their Limitations" in a book about the physics of baseball.

> In his analysis of a real system, a physicist constructs a well-defined model of the system and addresses the model. The system we address here is baseball. . . . We cannot calculate from first principles the character of the collision of an ash bat with a sphere made up of layers of different tightly wound yarns, nor do we have any precise understanding of the effect of the airstream on the flight of that sphere, with its curious yin-yang pattern of stitches. What we can do is construct plausible models of those interactions that play a part in baseball that do not violate basic principles of mechanics. Though these basic principles . . . severely constrain such models, they do not completely define them. It is necessary that the models touch the results of observations — or the results of the controlled observations called experiments — at some points so that the model can be more precisely defined and used to interpolate between known results, or to extrapolate from them. . . . If the model is well chosen, so as to represent the salient points of the real system adequately, conclusions derived from an analysis of the model can apply to the system to a useful degree. (Adair, 2002, pp. 1–2)

A modeling philosophy addresses the essential question: *Why are we modeling this problem, and what can we expect to learn from the model?* This question must be answered by each modeler,

because no model is complete or fully verifiable (Oreskes et al., 1994); instead, the best that can be done is to sanction the model. According to Winsberg (2010, p. 23):

> The sanctioning of simulations does not cleanly divide into verification and validation. In fact, simulation results are sanctioned all at once: simulationists try to maximize fidelity to theory, to mathematical rigor, to physical intuition, and to known empirical results. But it is the *simultaneous confluence* of these efforts, rather than the establishment of each one separately, that ultimately gives us confidence in the results.

PFC models for intact rock have been sanctioned by demonstrating that they match the response obtained during tension and compression tests of typical compact rocks. Further discussion of the sanctioning of PFC models is provided in Potyondy (2015), and further discussion of modeling philosophy is given in Starfield and Cundall (1988), Starfield (1997) and Nicolson et al. (2002).

2.0 PFC MATERIALS AND INTERFACE

A PFC material consists of rigid grains that interact at contacts (see Figure 3).[8] The grains of the PFC material can be either balls or clumps drawn from a general grain-size distribution. It is the type of contact model at the grain-grain contacts that defines the material as being linear, contact-bonded, parallel-bonded or flat-jointed. The linear material is a granular material, and the other materials are bonded materials. A smooth-jointed interface can be inserted into the bonded materials. A user-defined material can also be created. All materials are produced within a material vessel such that they form a homogeneous, isotropic and well-connected grain assembly with a specified non-zero material pressure. The PFC material is produced by the material-genesis procedures described in Section 0.

The PFC materials and interface are described in the remaining subsections. Each material and interface is defined by a set of material properties. These properties control the material-genesis procedure, install the desired contact model at selected contacts and assign contact-model properties. The properties common to all PFC materials are described in the first subsection. The linear material is described in the second subsection. A general description of the bonded materials is provided in the third subsection, and followed by descriptions of each bonded material, the user-defined material, and the smooth-jointed interface.

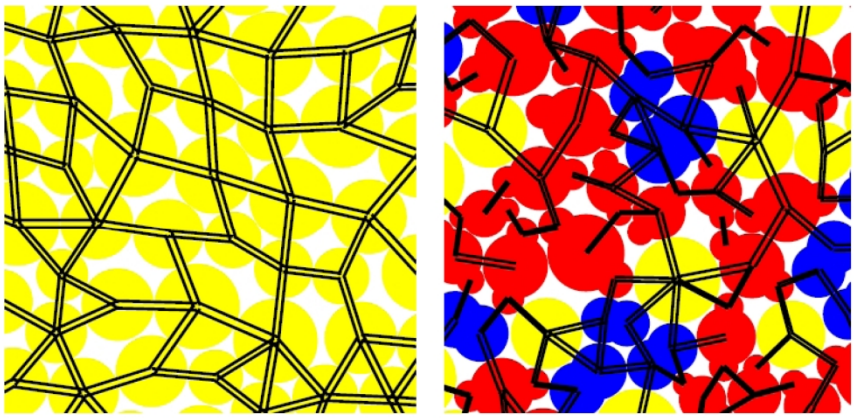

Figure 3 ***Bonded material consisting of grains (with balls in yellow and clumps in blue and red) and cement (drawn as pairs of black lines).*** (From Fig. 6 of Potyondy [2015].)

[8] The physical behavior at each contact is embodied in its contact model. For the bonded-particle materials, this physical behavior mimics cement, and thus, a bonded material has been said to consist of rigid grains joined by cement at grain-grain contacts. The PFC materials include a granular material along with the bonded materials; therefore, the present definition of a PFC material replaces "rigid grains joined by cement" with "rigid grains that interact at contacts."

2.1 Common Material Properties

The properties common to all PFC materials are described here and defined by the parameters listed in Table 1. The material name (N_{mt}) is used to create a model title that corresponds with the current state of the model. The material name (N_{ms}) is used to name the save states. The model title is displayed at the top of most views. The material type may be either one of the four supported materials or a user-defined material. Kinetic energy can be dissipated via local damping by specifying a non-zero value for the local-damping factor of each grain — quasi-static conditions are modeled by setting the local-damping factor to 0.7, and dynamic effects can be studied by choosing the local-damping factor to correspond with the seismic quality factor of the rock (Potyondy and Cundall, 2004, Eq. 3). The grain density is specified either directly or indirectly in terms of the bulk density. If the bulk density is given, then a single value of grain density is computed such that the mass of synthetic material will equal the bulk density times the vessel volume. The grain shape and size distribution are specified as follows. The grain shape must be either all balls or all clumps. If clumps are chosen, then a clump template must be provided for each clump shape. The size distribution is specified in terms of a finite number of separate size distributions, each of which is either uniform or Gaussian. The volume fraction and diameter range is given for each distribution.[9] The size distribution can be shifted by modifying the diameter multiplier — synthetic materials that differ only in their average grain diameter can be created by varying the diameter multiplier.

Table 1 Common Parameters

Parameter	Type	Range	Default	Description
N_{mt}, **cm_matName**	STR	NA	**PFCmat**	material name (for model title)
N_{ms}, **cm_matNameSAV**	STR	NA	**PFCmat**	material name (for SAV file names)
T_m, **cm_matType**	INT	$[0,4]$	0	material-type code 0, linear 1, contact-bonded 2, parallel-bonded 3, flat-jointed 4, user-defined
N_{cm}, **cm_modName**	STR	NA	NA	contact-model name ($T_m = 4$, also redefine **ft_setMatBehavior**)
α, **cm_localDampFac**	FLT	$[0.0,0.7]$	0.0	local-damping factor (for local damping)

[9] A given grain-size distribution (GSD) can be matched by specifying the volume fractions corresponding with the range of grain sizes — i.e., by breaking the given GSD into a finite number of uniform distributions (see Figure 14).

C_p , **cm_densityCode**	INT	$\{0,1\}$	0	density code $\begin{cases} 0, \text{ grain} \\ 1, \text{ bulk} \end{cases}$
ρ_v , **cm_densityVal**	FLT	$(0.0,\infty)$	NA	density value (set grain density: $\rho_g = \begin{cases} \rho_v, & C_\rho = 0 \\ \rho_v V_v / V_g, & C_\rho = 1 \end{cases}$ V_v is volume of vessel, and V_g is total volume of grains)
Grain shape & size distribution group:				
S_g , **cm_shape**	INT	$\{0,1\}$	0	grain-shape code $\begin{cases} 0, \text{ all balls} \\ 1, \text{ all clumps} \end{cases}$
n_{SD} , **cm_nSD**	INT	$n_{SD} \geq 1$	NA	number of size distributions
T_{SD} , **cm_typeSD(** n_{SD} **)**	STR	$\{0,1\}$	0	size-distribution type $\begin{cases} 0, \text{ uniform} \\ 1, \text{ gaussian} \end{cases}$
$N_{ct}^{(j)}$, **cm_ctName(** n_{SD} **)**	STR	NA	NA	clump-template name ($S_g = 1$)
$D_l^{(j)}$, **cm_Dlo(** n_{SD} **)**	FLT	$(0.0,\infty)$	NA	diameter range (lower)
$D_u^{(j)}$, **cm_Dup(** n_{SD} **)**	FLT	$D_u^{(j)} \geq D_l^{(j)}$	NA	diameter range (upper) (clumps: volume-equiv. sphere)
$\phi^{(j)}$, **cm_Vfrac(** n_{SD} **)**	FLT	$(0.0,1.0]$	NA	volume fraction $\left(\sum \phi^{(j)} = 1.0\right)$
D_{mult} , **cm_Dmult**	FLT	$(0.0,\infty)$	1.0	diameter multiplier (shifts the size distribution)

2.2 Linear Material

A linear material is a granular assembly in which the linear contact model exists at all grain-grain contacts at the end of the material-finalization phase; new grain-grain contacts that may form during subsequent motion are also assigned the linear contact model. A behavior summary of the linear contact model follows — refer to Itasca (2018)[10], for a comprehensive description of the model.

The linear model provides the behavior of an infinitesimal interface that does not resist relative rotation so that the contact moment equals zero ($\mathbf{M}_c \equiv 0$). The contact force is resolved into linear

[10] In documentation set at PFC: PFC Model Objects: Contacts and Contact Models: Contact Models: Built-in Contact Models: Linear Model.

and dashpot components ($\mathbf{F_c} = \mathbf{F^l} + \mathbf{F^d}$). The linear component provides linear elastic (no-tension), frictional behavior, while the dashpot component provides viscous behavior (see Figure 4). The linear force is produced by linear springs with constant normal and shear stiffnesses, k_n and k_s. The linear springs cannot sustain tension and slip is accommodated by imposing a Coulomb limit on the shear force using the friction coefficient, μ . The dashpot force is produced by dashpots with viscosity given in terms of the normal and shear critical-damping ratios, β_n and β_s. The linear springs act in parallel with the dashpots. The linear model with inactive dashpots and a reference gap of zero corresponds with the model of Cundall and Strack (1979).

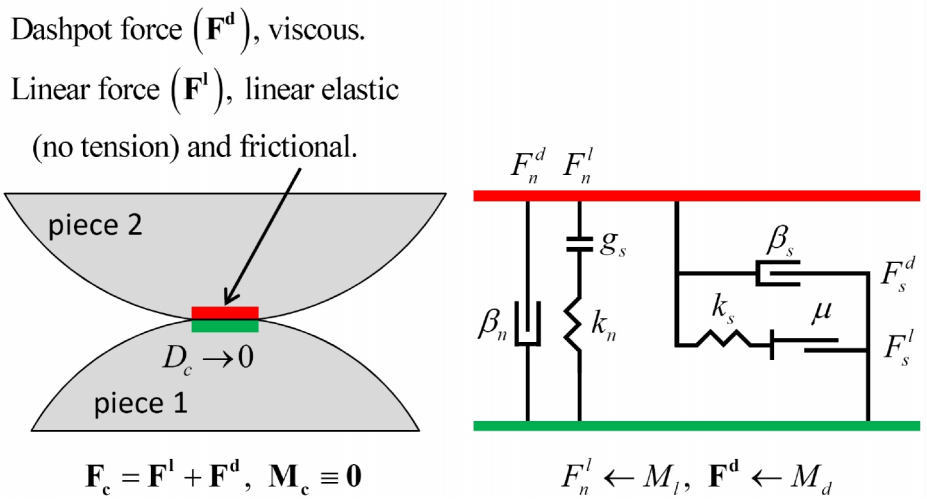

Figure 4 ***Behavior and rheological components of the linear model.*** (From Fig. 1 of Itasca [2018][11].)

A linear material is defined by the parameters in Table 2. The properties in the linear material group are used to set the relevant properties of the linear model during material finalization, and these same properties are assigned to grain-grain contacts during packing and that may form subsequent to material finalization.

The relevant properties of the linear model are as follows. The linear model provides linear and dashpot components. Only the linear component is active, the reference gap is zero and the normal-force update mode is absolute. The normal and shear stiffnesses are set based on a specified contact deformability (E^* and κ^* of the **deformability** method), and the friction coefficient is set to μ.

[11] In documentation set at PFC: PFC Model Objects: Contacts and Contact Models: Contact Models: Built-in Contact Models: Linear Model.

Table 2 Linear Material Parameters

Parameter	Type	Range	Default	Description
Material microproperties are listed via **`@mpListMicroProps`**. Common material parameters are listed in Table 1. Packing parameters are listed in Table 7.				
Linear material group:				
E^*, **`lnm_emod`**	FLT	$[0.0,\infty)$	0.0	effective modulus
κ^*, **`lnm_krat`**	FLT	$[0.0,\infty)$	0.0	stiffness ratio
μ, **`lnm_fric`**	FLT	$[0.0,\infty)$	0.0	friction coefficient

2.3 Bonded Materials

Bonded materials are analogous to intact rock, which can be viewed as an aggregate of crystals and amorphous particles joined by varying amounts of cementing materials. The bonded materials produced by the material-genesis procedure approximate an intact compact rock with average homogeneous isotropic properties at a scale larger than the material granularity. The synthetic material is analogous to brittle cookie dough that has been solidified by baking and for which grain size corresponds with dough granularity. The granularity is quantified by means of its resolution (or number of grains across a relevant dimension).

A rich variety of microstructures can be produced by modifying the bonded material itself. Such microstructures are obtained either by modifying the properties of the grains and cement or by modifying the packing fabric. The grain properties are size and shape. The cement properties are deformability and strength as well as evolving damage. The cement properties are embodied in the contact model, but the macroscopic material behavior is also sensitive to the ways in which new contacts form and contacts deemed to be broken behave. The packing fabric is affected by the size distribution and shapes of the grains as well as the material pressure. Structural features at a scale larger than the material granularity can be overlaid on the base material. These features include voids, material regions and joints (see Potyondy [2015]).

Damage in the bonded materials consists of bond-breakage events. In the contact- and parallel-bonded materials, the entire interface breaks, whereas in the flat-jointed material, the elements break. Each breakage event is denoted as a crack; thus, a fully broken interface in a 2D flat-joint contact with four elements contains four cracks. Cracks in the flat-jointed material are shown in Figure 10.

2.4 Contact-Bonded Material

A contact-bonded material is a granular assembly in which the linear contact bond contact model exists at all grain-grain contacts at the end of the material-finalization phase; new grain-grain contacts that may form during subsequent motion are assigned the linear contact model. A behavior summary of the linear contact bond contact model follows — refer to Itasca (2018)[12] for a comprehensive description of the model.

The linear contact bond model provides the behavior of an infinitesimal, linear elastic and either bonded or frictional interface that carries a force (see Figure 5). The interface does not resist relative rotation and is either bonded or unbonded. If bonded, the behavior is linear elastic until the strength limit is exceeded and the bond breaks making the interface unbonded. If unbonded, the behavior is linear elastic and frictional with slip being accommodated by imposing a Coulomb limit on the shear force. The unbonded linear contact bond model is equivalent to the linear model. The linear contact bond model with inactive dashpots and a reference gap of zero corresponds with the contact-bond model of Potyondy and Cundall (2004).

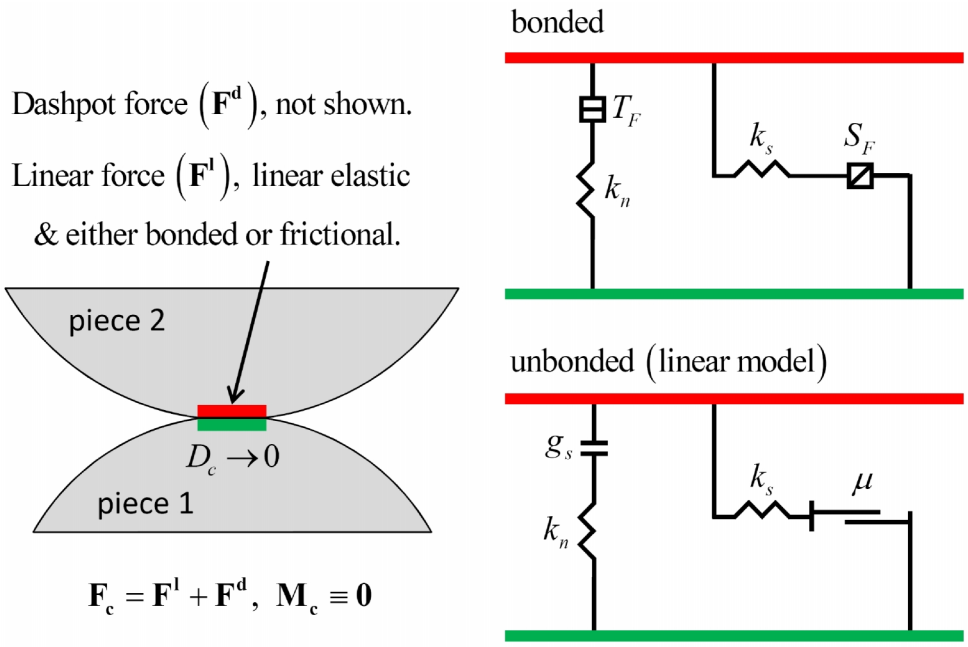

Figure 5 ***Behavior and rheological components of the linear contact bond model with inactive dashpots.*** (From Fig. 1 of Itasca [2018][13].)

[12] In documentation set at PFC: PFC Model Objects: Contacts and Contact Models: Built-in Contact Models: Contact Models: Linear Contact Bond Model.
[13] In documentation set at PFC: PFC Model Objects: Contacts and Contact Models: Contact Models: Built-in Contact Models: Linear Contact Bond Model.

A contact-bonded material is defined by the parameters in Table 3. The properties in the contact-bonded material group are used to set the relevant properties of the linear contact bond model during material finalization, and the properties in the linear material group are assigned to grain-grain contacts during packing and that may form subsequent to material finalization.

The relevant properties of the linear contact bond model are as follows. There are linear and dashpot components. Only the linear component is active. The reference gap is zero unless a bond is installed. If a bond is installed, then the reference gap is set equal to the contact gap at the time of bond installation (thereby establishing reference surfaces that are just touching and effectively removing the overlap or extending the grain surfaces). The normal-force update mode is absolute. The normal and shear stiffnesses are set based on a specified contact deformability (E^* and κ^* of the **deformability** method), and the friction coefficient is set to μ. Bonds are installed during material finalization at the grain-grain contacts with a gap less than or equal to the installation gap (g_i). The remaining properties correspond directly with properties in the contact-bond group of the linear contact bond model.

The relevant properties of the linear model are as follows. The linear model provides linear and dashpot components. Only the linear component is active, the reference gap is zero and the normal-force update mode is absolute. The normal and shear stiffnesses are set based on a specified contact deformability (E_n^* and κ_n^* of the **deformability** method), and the friction coefficient is set to μ_n.

Table 3 Contact-Bonded Material Parameters

Parameter	Type	Range	Default	Description
Material microproperties are listed via **`@mpListMicroProps`**. Common material parameters are listed in Table 1. Packing parameters are listed in Table 7.				
Contact-bonded material group:				
Linear group:				
E^*, **`cbm_emod`**	FLT	$[0.0,\infty)$	0.0	effective modulus
κ^*, **`cbm_krat`**	FLT	$[0.0,\infty)$	0.0	stiffness ratio
μ, **`cbm_fric`**	FLT	$[0.0,\infty)$	0.0	friction coefficient
Contact-bond group:				
g, **`cbm_igap`**	FLT	$[0.0,\infty)$	0.0	installation gap
$(T_\sigma)_{\{m,sd\}}$ **`cbm_tens_{m,sd}`**	FLT	$[0.0,\infty)$	$\{0.0,0.0\}$	tensile-strength dist. [stress] (mean and std. deviation)

$(S_\sigma)_{\{m,sd\}}$ **cbm_shears_{m,sd}**	FLT	$[0.0,\infty)$	$\{0.0,0.0\}$	shear-strength dist. [stress] (mean and std. deviation)
Linear material group (for grain-grain contacts during packing and that may form subsequent to material finalization)**:**				
E_n^*, **lnm_emod**	FLT	$[0.0,\infty)$	0.0	effective modulus
κ_n^*, **lnm_krat**	FLT	$[0.0,\infty)$	0.0	stiffness ratio
μ_n, **lnm_fric**	FLT	$[0.0,\infty)$	0.0	friction coefficient

2.5 Parallel-Bonded Material

A parallel-bonded material is a granular assembly in which the linear parallel bond contact model exists at all grain-grain contacts at the end of the material-finalization phase; new grain-grain contacts that may form during subsequent motion are assigned the linear contact model. A behavior summary of the linear parallel bond contact model follows — refer to Itasca (2018)[14] for a comprehensive description of the model.

The linear parallel bond model provides the behavior of two interfaces: an infinitesimal, linear elastic (no-tension) and frictional interface that carries a force and a finite-size, linear elastic and bonded interface that carries a force and moment (see Figure 6). The first interface is equivalent to the linear model: it does not resist relative rotation, and slip is accommodated by imposing a Coulomb limit on the shear force. The second interface is called a parallel bond, because when bonded, it acts in parallel with the first interface. When the second interface is bonded, it resists relative rotation, and its behavior is linear elastic until the strength limit is exceeded and the bond breaks making it unbonded. When the second interface is unbonded, it carries no load. The unbonded linear parallel bond model is equivalent to the linear model. The linear parallel bond model with inactive dashpots and a reference gap of zero corresponds with the parallel-bond model of Potyondy and Cundall (2004).

[14] In documentation set at PFC: PFC Model Objects: Contacts and Contact Models: Built-in Contact Models: Contact Models: Linear Parallel Bond Model.

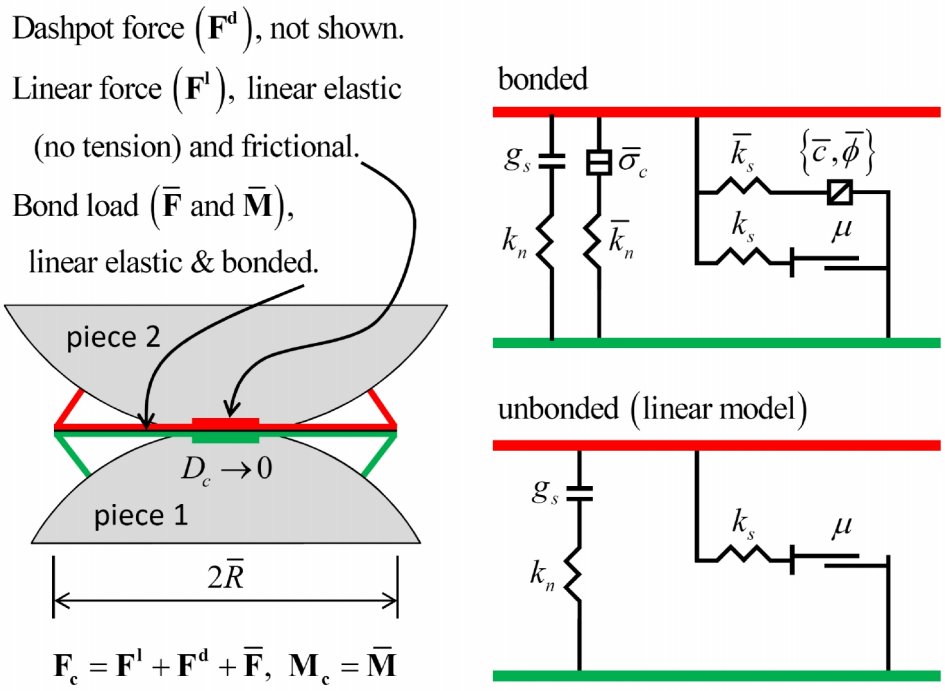

Figure 6 Behavior and rheological components of the linear parallel bond model with inactive dashpots. (From Fig. 1 of Itasca [2018][15].)

A parallel-bonded material is defined by the parameters in Table 4. The properties in the parallel-bonded material group are used to set the relevant properties of the linear parallel bond model during material finalization, and the properties in the linear material group are assigned to grain-grain contacts during packing and that may form subsequent to material finalization.

The relevant properties of the linear parallel bond model are as follows. The linear parallel bond model provides the behavior of two interfaces. The first interface is equivalent to the linear model, and the second interface is called a parallel bond.

- The relevant properties of the first interface are listed in the linear group. The first interface provides linear and dashpot components. Only the linear component is active. The reference gap is zero but may be altered when a bond is installed. If a bond is installed and the contact gap is negative, then the reference gap is set equal to the contact gap at the time of bond installation (thereby establishing reference surfaces that are just touching and effectively removing the overlap). The normal-force update mode is absolute. The normal and shear stiffnesses of the first interface are set based on a specified contact deformability (E^* and κ^* of the **deformability** method), and the friction coefficient is set to μ.

[15] In documentation set at PFC: PFC Model Objects: Contacts and Contact Models: Contact Models: Built-in Contact Models: Linear Parallel Bond Model.

- The relevant properties of the second interface are listed in the parallel-bond group. The second interface carries load only when it is bonded. Bonds are installed during material finalization at the grain-grain contacts with a gap less than or equal to the installation gap (g_i). The normal and shear stiffnesses of the second interface are set based on a specified deformability ($\bar{E}^*$ and $\bar{\kappa}^*$ of the **pb_deformability** method). The remaining properties of the second interface correspond directly with properties in the parallel-bond group of the linear parallel bond model.

The relevant properties of the linear model are as follows. The linear model provides linear and dashpot components. Only the linear component is active, the reference gap is zero and the normal-force update mode is absolute. The normal and shear stiffnesses are set based on a specified contact deformability (E_n^* and κ_n^* of the **deformability** method), and the friction coefficient is set to μ_n.

Table 4 Parallel-Bonded Material Parameters

Parameter	Type	Range	Default	Description
Material microproperties are listed via **`@mpListMicroProps`**. Common material parameters are listed in Table 1. Packing parameters are listed in Table 7.				
Parallel-bonded material group:				
Linear group:				
E^*, **pbm_emod**	FLT	$[0.0,\infty)$	0.0	effective modulus
κ^*, **pbm_krat**	FLT	$[0.0,\infty)$	0.0	stiffness ratio
μ, **pbm_fric**	FLT	$[0.0,\infty)$	0.0	friction coefficient
Parallel-bond group:				
g, **pbm_igap**	FLT	$[0.0,\infty)$	0.0	installation gap
$\bar{\lambda}$, **pbm_rmul**	FLT	$(0.0,\infty)$	1.0	radius multiplier
$\bar{E}^*$, **pbm_bemod**	FLT	$[0.0,\infty)$	0.0	bond effective modulus
$\bar{\kappa}^*$, **pbm_bkrat**	FLT	$[0.0,\infty)$	1.0	bond stiffness ratio
$\bar{\beta}$, **pbm_mcf**	FLT	$[0.0,1.0]$	0.0	moment-contribution factor
$(\bar{\sigma}_c)_{\{m,sd\}}$ **pbm_ten_{m,sd}**	FLT	$[0.0,\infty)$	$\{0.0,0.0\}$	tensile-strength dist. [stress] (mean and std. deviation)
$(\bar{c})_{\{m,sd\}}$	FLT	$[0.0,\infty)$	$\{0.0,0.0\}$	cohesion dist. [stress] (mean and std. deviation)

pbm_coh_{m,sd}				
$\bar{\phi}$, **pbm_fa**	FLT	$[0.0, 90.0)$	0.0	friction angle [degrees]
Linear material group (for grain-grain contacts during packing and that may form subsequent to material finalization)**:**				
E_n^*, **lnm_emod**	FLT	$[0.0, \infty)$	0.0	effective modulus
κ_n^*, **lnm_krat**	FLT	$[0.0, \infty)$	0.0	stiffness ratio
μ_n, **lnm_fric**	FLT	$[0.0, \infty)$	0.0	friction coefficient

2.6 Flat-Jointed Material

A flat-jointed material is a granular assembly in which the flat-joint contact model exists at all grain-grain contacts with a gap less than or equal to the installation gap at the end of the material-finalization phase; all other grain-grain contacts as well as new grain-grain contacts that may form during subsequent motion are assigned the linear contact model. A behavior summary of the flat-joint contact model follows — refer to Itasca (2018)[16] for a comprehensive description of the model. A high-level description of a flat-jointed material is provided in Section 2.6.1. The model is applied to study sandstone perforation failure in Potyondy (2017), and match the compressive to tensile strength ratio of Lac du Bonnet granite in Potyondy (2018).

The flat-joint model provides the macroscopic behavior of a finite-size, linear elastic and either bonded or frictional interface that may sustain partial damage (see Figure 7). The interface is discretized into elements. Each element is either bonded or unbonded, and the breakage of each bonded element contributes partial damage to the interface. The behavior of a bonded element is linear elastic until the strength limit is exceeded and the bond breaks making the element unbonded, while the behavior of an unbonded element is linear elastic and frictional with slip accommodated by imposing a Coulomb limit on the shear force. Each element carries a force and moment that obey the force-displacement law described below, while the force-displacement response of the flat-joint interface is an emergent behavior that includes evolving from a fully bonded state to a fully unbonded and frictional state.

[16] In documentation set at PFC: PFC Model Objects: Contacts and Contact Models: Contact Models: Built-in Contact Models: Flat-Joint Model.

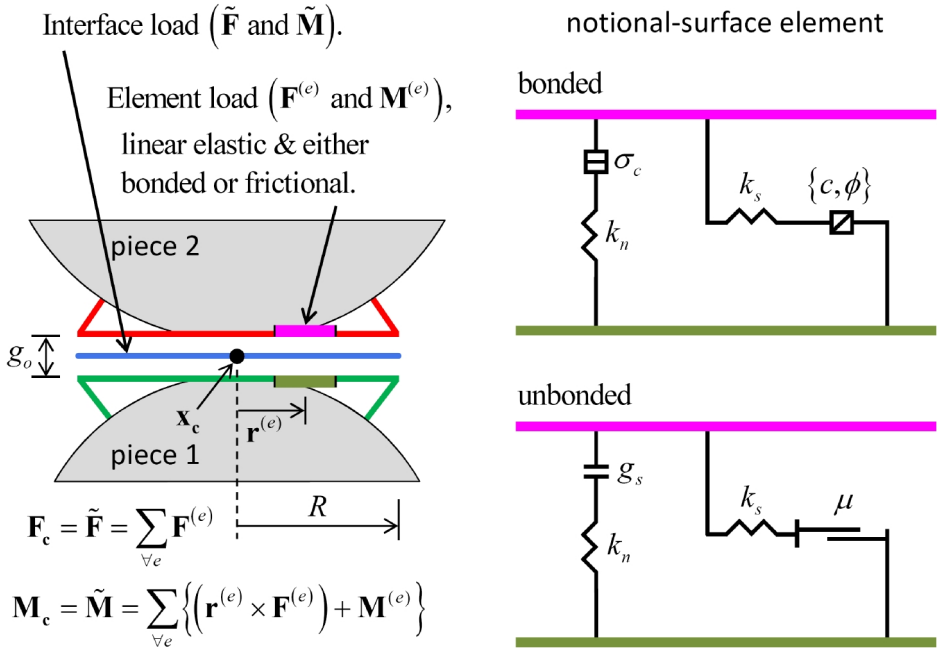

Figure 7 ***Behavior and rheological components of the flat-joint model.*** (From Fig. 8 of Itasca [2018][17].)

A flat-jointed material is defined by the parameters in Table 5. The properties in the flat-jointed material group are used to set the relevant properties of the flat-joint model during material finalization, and the properties in the linear material group are assigned to grain-grain contacts during packing and that may form subsequent to material finalization.

The relevant properties of the flat-joint model are as follows. The flat-joint contact model is installed at all grain-grain contacts with a gap less than or equal to the installation gap (g_i). The normal and shear stiffnesses are set based on a specified deformability (E^* and κ^* of the **deformability** method). The property set $\left\{\phi_B, \phi_G, (g_o)_{\{\text{m,sd}\}}, C_\lambda, \lambda_v\right\}$ is described in Section 2.6.2. The remaining properties correspond directly with properties of the flat-joint model

The relevant properties of the linear model are as follows. The linear model provides linear and dashpot components. Only the linear component is active, the reference gap is zero and the normal-force update mode is absolute. The normal and shear stiffnesses are set based on a specified contact deformability (E_n^* and κ_n^* of the **deformability** method), and the friction coefficient is set to μ_n.

[17] In documentation set at PFC: PFC Model Objects: Contacts and Contact Models: Contact Models: Built-in Contact Models: Flat-Joint Contact Model.

Table 5 Flat-Jointed Material Parameters

Parameter	Type	Range	Default	Description
Material microproperties are listed via **`@mpListMicroProps`**. Common material parameters are listed in Table 1. Packing parameters are listed in Table 7.				
Flat-jointed material group:				
C_{MS}, **`fjm_trackMS`**	BOOL	$\{\text{true}, \text{false}\}$	false	microstructure-tracking flag (draw microstructure with the faced grain plot set)
g_i, **`fjm_igap`**	FLT	$[0.0, \infty)$	0.0	installation gap
ϕ_B^+, **`fjm_B_frac`**	FLT	$[0.0, 1.0]$	NA	bonded fraction
ϕ_G^+, **`fjm_G_frac`**	FLT	$[0.0, 1.0]$	NA	gapped fraction
$(g_o)_{\{m,sd\}}$, **`fjm_G_{m,sd}`**	FLT	$[0.0, \infty)$	$\{0.0, 0.0\}$	initial surface-gap distribution (mean and std. deviation)
N_r, **`fjm_Nr`**	INT	$[1, \infty)$	2	elements in radial direc. (2D model: total elements)
N_α, **`fjm_Nal`**	INT	$[3, \infty)$	4	elements in circumf. direc. (3D model only)
C_λ, **`fjm_rmulCode`**	INT	$\{0, 1, 2\}$	0	radius-multiplier code $\begin{cases} 0, & \lambda \text{ constant (no valid check)} \\ 1, & \text{valid } (\lambda \text{ non-uniform reduce}) \\ 2, & \text{valid } (\lambda \text{ uniform reduce}) \end{cases}$
λ_v, **`fjm_rmulVal`**	FLT	$(0.0, \infty)$	1.0	radius-multiplier value $\lambda = \lambda_v = \begin{cases} \lambda_f, & C_\lambda = 0 \\ \lambda_o, & C_\lambda = \{1, 2\} \end{cases}$ λ_f is fixed value, and λ_o is starting value
E^*, **`fjm_emod`**	FLT	$[0.0, \infty)$	0.0	effective modulus
κ^*, **`fjm_krat`**	FLT	$[0.0, \infty)$	0.0	stiffness ratio
μ, **`fjm_fric`**	FLT	$[0.0, \infty)$	0.0	friction coefficient
$(\sigma_c)_{\{m,sd\}}$ **`fjm_ten_{m,sd}`**	FLT	$[0.0, \infty)$	$\{0.0, 0.0\}$	tensile-strength dist. [stress] (mean and std. deviation)
$(c)_{\{m,sd\}}$ **`fjm_coh_{m,sd}`**	FLT	$[0.0, \infty)$	$\{0.0, 0.0\}$	cohesion dist. [stress] (mean and std. deviation)

ϕ, **fjm_fa**	FLT	$[0.0, 90.0)$	0.0	friction angle [degrees]
Linear material group (for grain-grain contacts during packing, that are not flat-jointed, and that may form subsequent to material finalization):				
E_n^*, **lnm_emod**	FLT	$[0.0, \infty)$	0.0	effective modulus
κ_n^*, **lnm_krat**	FLT	$[0.0, \infty)$	0.0	stiffness ratio
μ_n, **lnm_fric**	FLT	$[0.0, \infty)$	0.0	friction coefficient

+ Slit fraction: $\phi_S = 1 - \phi_B - \phi_G \quad (0 \le \phi_S \le 1)$.

2.6.1 High-Level Description of Flat-Jointed Material

A flat-joint contact and its corresponding flat-jointed material are shown in Figure 8. A flat-joint contact simulates the behavior of an interface between two notional surfaces, each of which is connected rigidly to a piece of a body. A flat-jointed material consists of bodies (balls, clumps or walls) joined by flat-joint contacts such that the effective surface of each body is defined by the notional surfaces of its pieces, which interact at each flat-joint contact with the notional surface of the contacting piece. The notional surfaces are called faces, which are lines in 2D and disks in 3D.

The following description of a flat-jointed material applies to the case in which bodies are balls; however, the flat-joint model can be installed at both ball-ball and ball-wall contacts. We refer to the balls of a flat-jointed material as faced grains, each of which is depicted as a circular or spherical core and a number of skirted faces. The faced grains are created when the flat-joint model is installed at the ball-ball contacts of a packed ball assembly (see Figure 9). An interface exists between each set of adjoining faces and is discretized into elements with each element being either bonded or unbonded. The breakage of each bonded element contributes partial damage to the interface, and each breakage event is denoted as a crack (see Figure 10).[18] If the relative displacement at a flat-joint contact becomes larger than the flat-joint diameter, then the adjoining faces may be removed (because the contact may be deleted) making the associated balls locally circular or spherical; if these balls come back into contact, the behavior will be that of an interface between circular or spherical surfaces (if the linear contact model is assigned to the new contact).

[18] Cracks in the 2D flat-jointed material are depicted as colored lines lying on the interface between the two disk-shaped pebbles with color denoting breakage mode and with line thickness proportional to the element gap. Cracks in the 3D flat-jointed material are depicted as colored octagons lying on the interface between the two spherical pebbles with color denoting breakage mode.

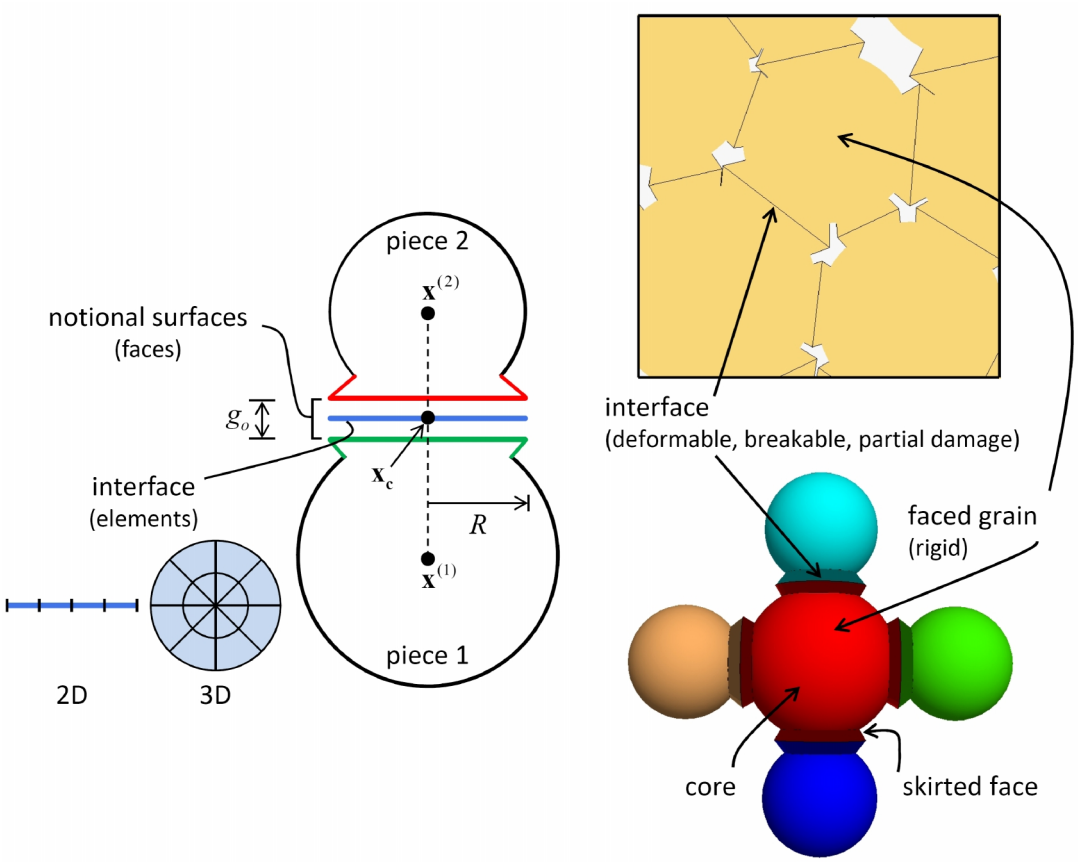

Figure 8 ***Flat-joint contact (left) and flat-jointed material (right).*** (From Fig. 1 of Itasca [2018][19].)

[19] In documentation set at PFC: PFC Model Objects: Contacts and Contact Models: Contact Models: Built-in Contact Models: Flat-Joint Contact Model.

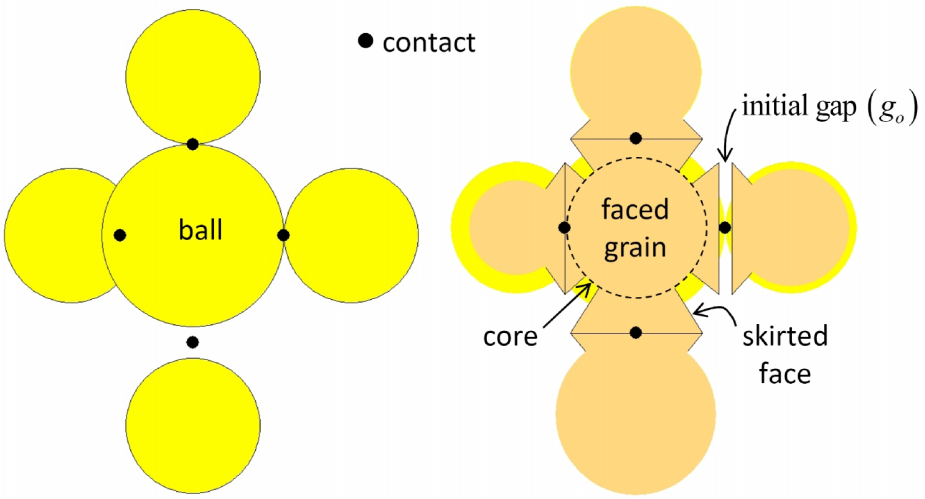

Figure 9 ***Creation of faced grains showing packed ball assembly (left) and initial faced-grain assembly (right).*** (From Fig. 2 of Itasca [2018][20].)

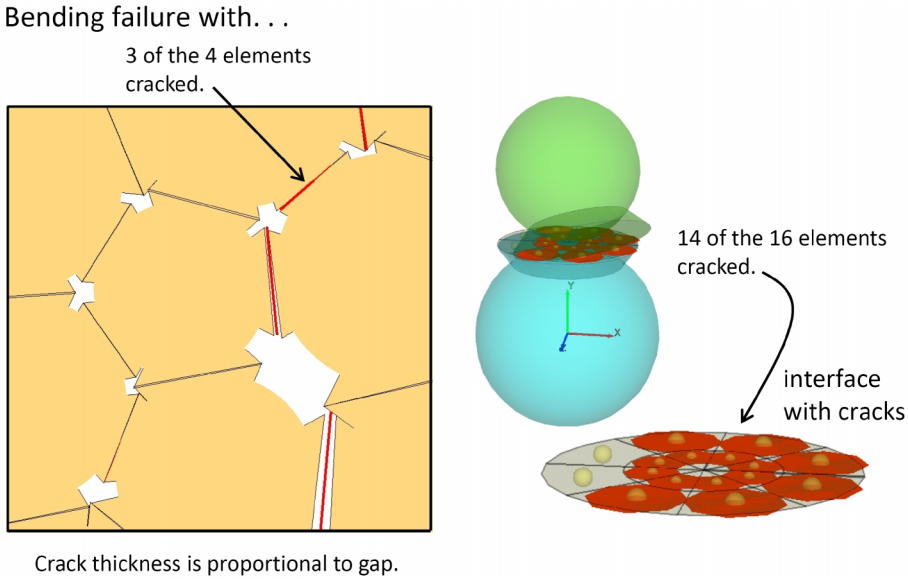

Figure 10 ***Partially damaged flat-jointed material showing faced grains with cracks colored red/blue for tensile/shear failure.*** (From Fig. 3 of Itasca [2018][21].)

2.6.2 Flat-Jointed Material Microstructure

The microstructure of a flat-jointed material (see Figure 11) is such that each flat-joint contact is initially either bonded ($g_o = 0$, bonded), gapped ($g_o > 0$, unbonded) or slit ($g_o = 0$, unbonded). This

[20] In documentation set at PFC: PFC Model Objects: Contact and Contact Models: Contact Models: Built-in Contact Models: Flat-Joint Contact Model.
[21] In documentation set at PFC: PFC Model Objects: Contact and Contact Models: Contact Models: Built-in Contact Models: Flat-Joint Contact Model.

information is stored in the property 'fj_mtype' of each flat-jointed contact. The material microstructural parameters are the fraction of bonded and gapped contacts (ϕ_B and ϕ_G), and the mean and standard deviation of the initial gap for the gapped contacts ($(g_o)_{\{msd\}}$). When the flat-jointed material is created, each flat-joint contact is designated as being of type B, G or S (as described below), and the type G contacts are assigned an initial gap drawn from a normal distribution with the specified mean and standard deviation. The initial microstructural types of the flat-jointed material are computed and listed by **`mpListMicroStrucProps`**, which returns the number of flat-joints initially bonded (**`mp_nFJiB`**), gapped (**`mp_nFJiG`**), slit (**`mp_nFJiS`**) or undefined (**`mp_nFJiU`**).

The following type-designation process is applied to the set of flat-joint contacts. Denote the fractions of bonded, gapped and slit contacts as ϕ_B, ϕ_G and ϕ_S, respectively. These fractions are related to the number of bonded, gapped and slit contacts (n_B , n_G and n_S , respectively) as well as the total number of flat-joint contacts (n_{FJ}) by the relations:

$$\phi_B = \frac{n_B}{n_{\text{FJ}}}, \quad \phi_G = \frac{n_G}{n_{\text{FJ}}}, \quad \phi_S = \frac{n_S}{n_{\text{FJ}}}$$
$$\phi_B + \phi_G + \phi_S = 1 \quad \text{and} \quad n_{\text{FJ}} = n_B + n_G + n_S . \tag{1}$$

The microstructural types are assigned by looping through the set of flat-joint contacts. The first n_B of these contacts are designated as type B, the next n_G of these contacts are designated as type G and the remaining n_S of these contacts are designated as type S. The type designations are spatially random, because the contact list is spatially random (which is assumed to be the case).

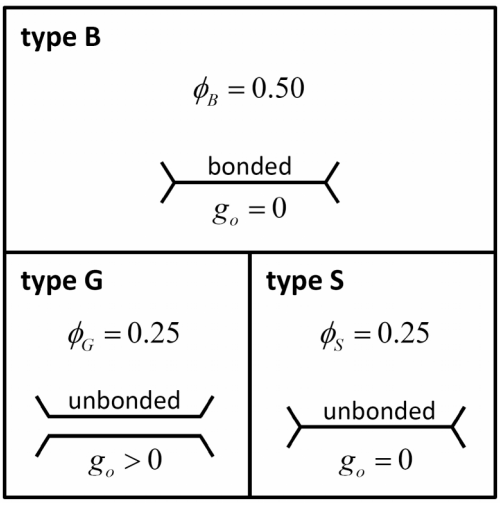

Figure 11 Initial microstructure of flat-jointed material: each flat-joint contact is bonded (type B), gapped (type G) or slit (type S).

Microstructural validity describes whether or not the grain facets overlap one another; a flat-jointed material has a valid microstructure if and only if the facets of each grain can be connected to the grain center with no overlap.[22] Microstructural validity is controlled as follows (see Figure 12). The radius multipliers of a flat-jointed material can either be fixed $(C_\lambda = 0)$ or reduced $(C_\lambda = 1 \text{ or } 2)$ to obtain a valid microstructure. If the multipliers are fixed, then all flat-joint radius multipliers are set equal to the specified value, and no validity check is performed. The multipliers can be reduced either uniformly or non-uniformly until all faced grains have a valid microstructure. The non-uniform reduction algorithm visits the flat-jointed contacts of each ball in the model. The flat-jointed contacts of a given ball are compared with one another, and those whose facets overlap have their flat-joint radii reduced uniformly until they no longer overlap.

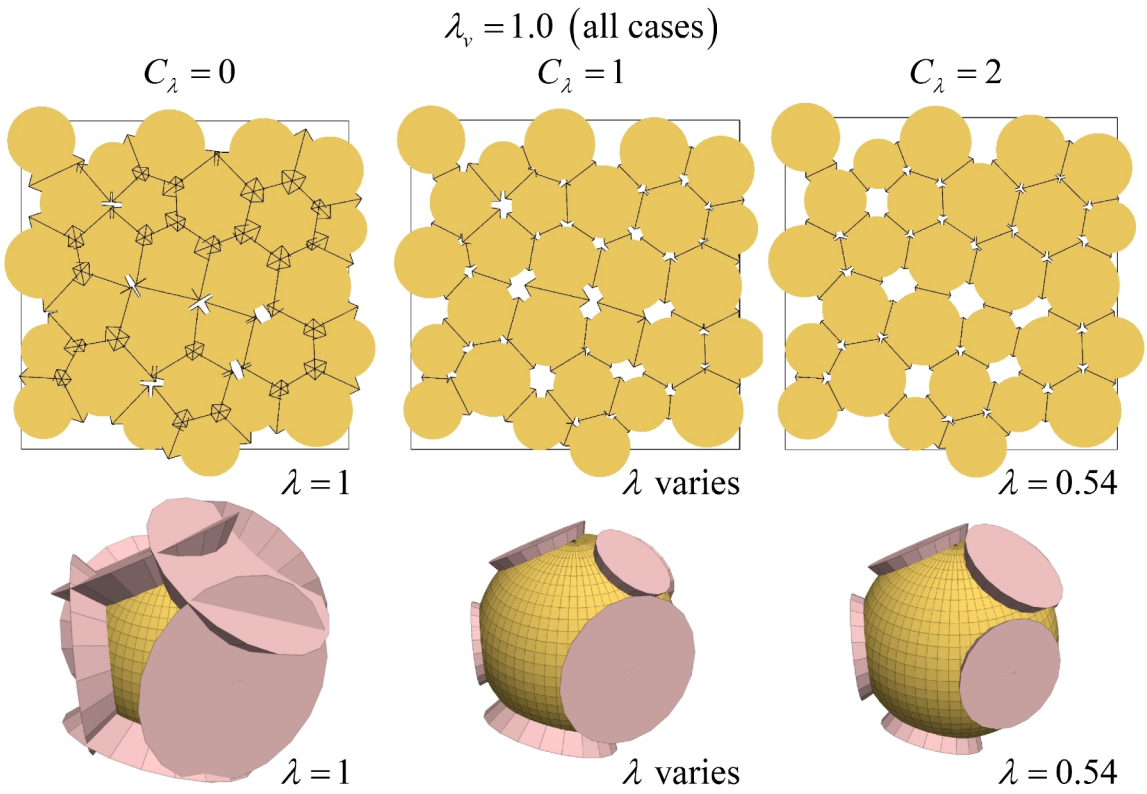

Figure 12 ***The three types of flat-jointed microstructures produced by the material-modeling support package. The left-most images have invalid microstructures, while the middle and right images have valid microstructures. Only a single faced grain is shown for the 3D case (bottom).***

[22] A microstructurally invalid model may produce useful behavior, and as such, its use can be justified — parallel-bonded materials with radius multipliers of unity have invalid microstructures.

2.7 User-Defined Material

A user-defined material is a granular assembly in which a user-defined contact model exists at all grain-grain contacts. The user-defined contact model is referred to in commands and FISH by the contact-model name (N_{cm} in Table 1), and is provided as a dynamic link library (DLL) file that is loaded into PFC at runtime. The user-defined material example creates a 3D hill material that uses the hill contact model by specifying the contact-model name as **`hill`**. The user-defined material is defined by a set of parameters that are used to set the relevant properties of the contact model during material genesis and subsequent modeling — the properties are specified in the redefinition of the **`ft_setMatBehavior`** FISH function. The following additional FISH functions must also be provided for a user-defined material: **`udm_checkParams`**, **`udm_listProps`**, **`udm_computeMicroStrucProps`**, and **`udm_listMicroStrucProps`**. Refer to the user-defined material example for more information about how to create a user-defined material.

2.8 Smooth-Jointed Interface

A smooth-jointed interface can be inserted into the bonded materials by identifying the contacts near the interface and replacing their contact models with the smooth-joint contact model. New grain-grain contacts that may form during subsequent motion are assigned the linear contact model, with the exception of the new contacts associated with the interface, which are assigned the smooth-joint contact model and aligned with the interface direction. This capability is not provided in the material-modeling support package, but it is relatively straightforward to perform this operation as described in Itasca (2018).[23]

[23] In documentation set at Examples: PFC Examples: Tutorials: Slip on a Fault.

3.0 MICROSTRUCTURAL MONITORING

The macroscopic behavior of the synthetic material arises from the evolution of the microstructural features. Microstructural monitoring includes computation of quantitative microstructural properties, microstructural plot sets, force-chain fabric and crack monitoring. These items are described in the following four subsections.

3.1 Microstructural Properties

The microstructural properties of the material are computed and listed by **`mpListMicroStrucProps`** and include the following items.

- **Grain Size and Packing Information.** Number of grains in the model, grain-size distribution (discussed below), average and median grain diameters, vessel resolutions w.r.t. the average and median grain diameters,[24] measurement-based porosity (defined in Section 5.1), and overlap ratios.[25]
- **Contact Information.** The number of active linear-based contacts along with the number of such contacts that are grain-grain and grain-wall.
- **Bonded-Material Information.** The bonded materials provide this information. Bond coordination number (c_b).[26] Number of contact-bonded bonds, parallel-bonded bonds, flat-jointed contacts, flat-jointed elements, and flat-jointed bonds. The initial microstructural types of the flat-jointed material (defined in Section 2.6.2).
- **User-Defined Material Information.** A user-defined material may provide this information via **`udm_{compute,list}MicroStrucProps`**.

The cumulative distribution of grain size is most often used to characterize particulate media (Santamarina et al., 2001). The typical grain size distribution curve is a cumulative distribution of mass according to particle size — it is NOT a cumulative distribution of particle counts. The curve expresses the mass percentage of particles that can pass through a given sieve size. The horizontal axis is particle size, and the vertical axis is "mass percent passing." A typical grain size distribution curve is shown in Figure 13. If the vertical axis is labelled "percent finer than," then it is understood that this denotes the percentage by mass, not the percentage by number. The equivalent particle sizes corresponding to selected percentiles are frequently quoted. For example, d_{50} corresponds to the sieve size that 50 percent of the particles can pass through (and these particles comprise 50 percent of the total mass), and d_{10} corresponds to the sieve size that 10 percent of the particles can pass

[24] Vessel resolution is defined as the number of grains across the minimum vessel dimension.
[25] The overlap ratios (ORs) of all active contacts are computed, and the maximum, minimum and average values are returned. The OR is the overlap divided by the piece diameter. For grain-grain contacts, there are two ORs, while for grain-wall contacts, there is one OR.
[26] The bond coordination number is defined for the bonded materials as the average number of intact bonds per grain.

through (and these particles comprise 10 percent of the total mass). The quantity d_{50} is called the median grain size. The slope of the cumulative distribution and its convexity or concavity are characterized by the coefficients of uniformity C_u and curvature C_c:

$$C_u = \frac{d_{60}}{d_{10}} \quad \text{and} \quad C_c = \frac{d_{30}^2}{d_{10} d_{60}}. \tag{2}$$

A well-graded material with $C_u > 4$ indicates that there are large particles forming the soil frame and that voids are filled with smaller particles, potentially forming a dense soil mass.

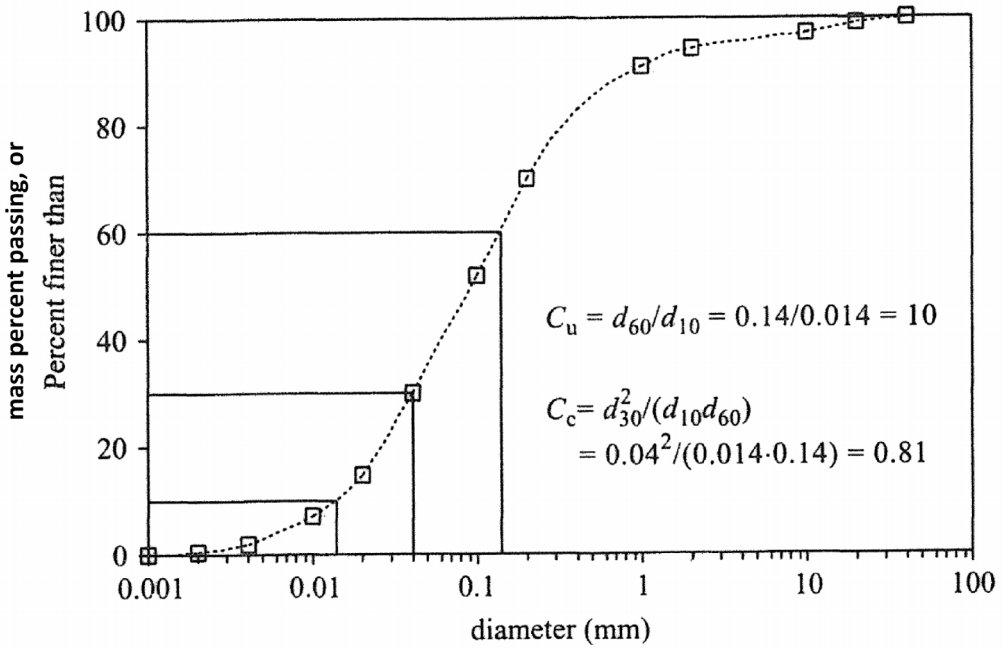

Figure 13 ***Typical grain size distribution curve showing the cumulative distribution of mass according to particle size.*** (From Fig. 2.10 of Santamarina et al. [2001].)

The grain size distribution (GSD) for a sample of the synthetic material is computed via **`@gsdMeasure(n)`**, where **`n`** is the number of bins over which the GSD is sampled, and the sampled grains are defined by **`@gsdMark`** (see Figure 14). The GSD is returned in a table named 'GSD' for which the x-axis is the effective grain diameter and the y-axis is the cumulative mass percent passing. A table named 'GSD-retained' is also created for which the x-axis is the effective grain diameter and the y-axis is the incremental mass percent retained. The cumulative mass percent passing curve corresponds with the typical grain size distribution curve shown in Figure 13. The incremental mass percent retained histogram corresponds with the material retained on each sieve during a sieve analysis. The grain size for percentile **`pct`** is extracted from the table named 'GSD'

via **`@gsdGetSizeOfPercentile(pct)`**. For circular and spherical grains, the grain mass is given by

$$M_g = \rho_g V_g, \quad V_g = \begin{cases} \pi\left(\dfrac{D_g}{2}\right)^2 t, & \text{2D } (t=1) \\ \dfrac{4}{3}\pi\left(\dfrac{D_g}{2}\right)^3, & \text{3D} \end{cases} \tag{3}$$

where ρ_g is grain density, V_g is grain volume and D_g is grain diameter.[27] Some of the grain size distribution information can be obtained by the measurement logic.[28]

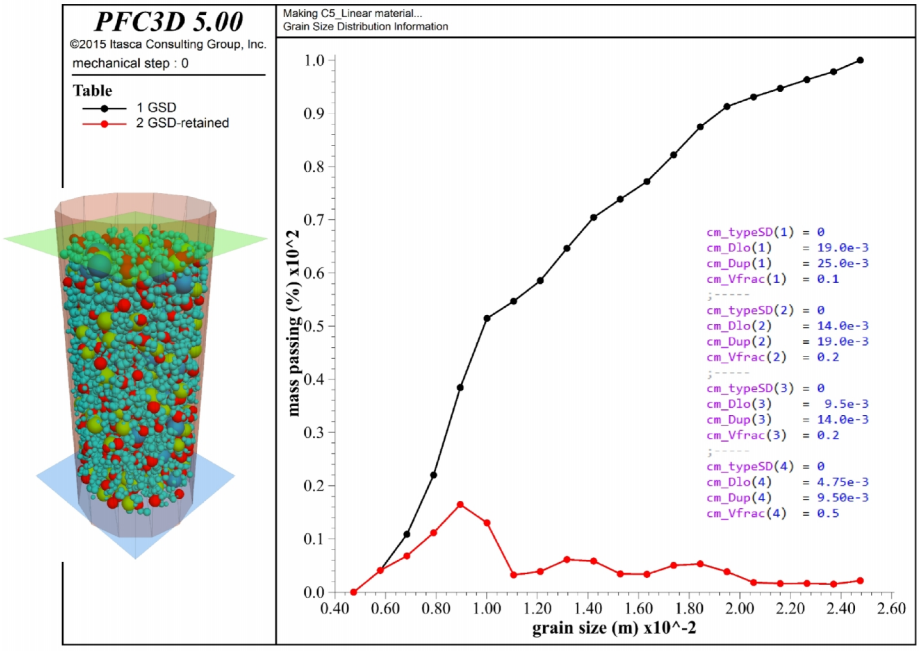

Figure 14 Grain size distribution information produced by the FISH function gsdMeasure(19) showing cumulative mass percent passing (in black) and incremental mass percent retained (in red).

[27] The current fistPkg supports circular and spherical grain shapes by considering such grains as balls. The fistPkg will support general grain shapes by considering such grains as clumps (by setting $S_g = 1$ in Table 1, and providing a clump template for each shape).

[28] The cumulative volume percent passing curve can be obtained with the measurement logic (by specifying the number of bins and the grain-diameter range for the size-distribution computation when creating a measurement sphere with the **`measure create`** command, and extracting the information into a table with the **`measure dump`** command). If all sampled grains have the same density, then the cumulative volume percent passing curve is equal to the cumulative mass percent passing curve.

3.2 Microstructural Plot Sets

Microstructural plot sets are provided for the bonded materials to display the material microstructure and thereby reveal how the evolution of the microstructure influences the macroscopic behavior. The microstructural plot sets include depictions of the grains and the grain-grain interfaces, and when used with the crack-monitoring package, include the interface damage in the form of bond breakages.

A plot set is defined as a plot in which the plot information is stored as a geometry set and displayed by the geometry set plot item by specifying: {ColorBy: Set}, and {Sets: <geometry set name>}. The microstructural plot set capability is activated via **`msOn`**, the plot sets are regenerated at a specified rate (**`msUpdateRate`**) during cycling, and the regeneration can be forced to occur via **`msForceUpdate`**. An axis-aligned microstructural box (defined by **`msBoxDefine`**) is associated with the microstructural plot sets. The box is displayed by the geometry set plot item by specifying: {ColorBy: Set}, and {Sets: msBox}. The grains with centers inside the box can be displayed with either: (a) the ball and clump plot items by specifying: {Color By: Text Val: msBox}, or (b) the grain and faced grain plot sets. The contact-based plot sets display only the entities joining the grains in the box. The faced grain plot set displays only the faces joining grains with centers inside the box. The following microstructural plot sets are available: grains, contact bonds, pbond interfaces, pbond cement, FJ interfaces, faced grains and cracks (see Figures 15 to 18).

Grains. A contact- or parallel-bonded material mimics the microstructure of rigid ball- or clump-shaped grains cemented with either spot welds or epoxy. The grain plot set (geometry set name: **"grains"**) displays each grain as a sphere — only ball-shaped grains are displayed, clump-shaped grains are not supported. The sphere is centered at the ball location and has radius equal to the scale factor (**`msGN_sfacRad`**) times the ball radius. For the 2D model, the grains are displayed as circles.

Contact bonds. A contact-bonded material mimics the microstructure of rigid grains cemented with spot welds. The contact bond plot set (geometry set name: **"contact bonds"**) displays each intact grain-grain contact bond as a line. The line is centered at the contact location and has length equal to the scale factor (**`msCB_sfacLen`**) times the distance between the centers of the two contacting pieces.

Parallel bonds. A parallel-bonded material mimics the microstructure of rigid grains cemented with epoxy. There are two plots sets. The first plot set depicts the parallel bond as an interface, while the second plot set depicts the parallel bond as cement.

The parallel-bond interfaces plot set (geometry set name: **"pbond interfaces"**) displays each intact grain-grain parallel bond as a disk with radius equal to the scale factor (α,

msPBi_sfacRad) times the parallel-bond radius $\left(\overline{R}\right)$. The disk is centered at the contact location and lies on the contact plane. For the 2D model, the parallel-bond interfaces are displayed as lines (of length $2\alpha\overline{R}$, and unit-thickness depth).

The parallel-bond cement plot set (geometry set name: **"pbond cement"**) displays each intact grain-grain parallel bond as a cylinder with radius equal to the scale factor (α, **msPBc_sfacRad**) times the parallel-bond radius $\left(\overline{R}\right)$. The cylinder is centered at the contact location and has a length $\left(L\right)$ equal to the scale factor (**msPBc_sfacLen**) times the distance between the centers of the two contacting pieces. For the 2D model, the parallel-bond cement is displayed as a thick line (of length L, thickness $2\alpha\overline{R}$, and unit-thickness depth).

Flat-Jointed Material. A flat-jointed material mimics the microstructure of rigid faced grains with bonded and frictional interfaces. There are two plots sets. The first plot set depicts the interfaces, while the second plot set depicts the faced grains.

The flat-joint interfaces plot set (geometry set name: **"FJ interfaces"**) displays the interface of each grain-grain flat-jointed contact. The interface, coordinate systems and discretization can be displayed by the geometry set plot item by specifying {ColorBy: Group} and {Sets: FJ interfaces}, with {Color-List:} used to turn each entity on/off and specify its color. The visualization scheme for each entity is as follows.

a. **Interface** (group 'interface'). The interface is drawn as a disk with radius equal to the scale factor (α, **msFJi_sfacRad**) times the flat-joint radius $\left(R\right)$. The disk is centered at the contact location and lies on the contact plane. For the 2D model, the flat-joint interfaces are displayed as lines (of length $2\alpha R$, and unit-thickness depth).
b. **Coordinate systems** (groups 's-tSys' and 'xi-etaSys'). The two coordinate systems associated with the interface (nst) and ($n\xi\eta$) are drawn as lines from interface center extending just beyond the interface edge, with the lines in the s and ξ directions being shorter than the lines in the t and η directions. For the 2D model, the group is 'n-tSys', and only the n and t directions of the nst coordinate system are drawn.
c. **Discretization** (group 'elements'). The interface discretization shows elements and centroid locations. The outline of each element is drawn as a set of edges, and there is a short line (aligned with the s direction) at each element centroid. For the 2D model, each element is outlined by edges oriented perpendicular to the interface, with a shorter perpendicular line at each element centroid.

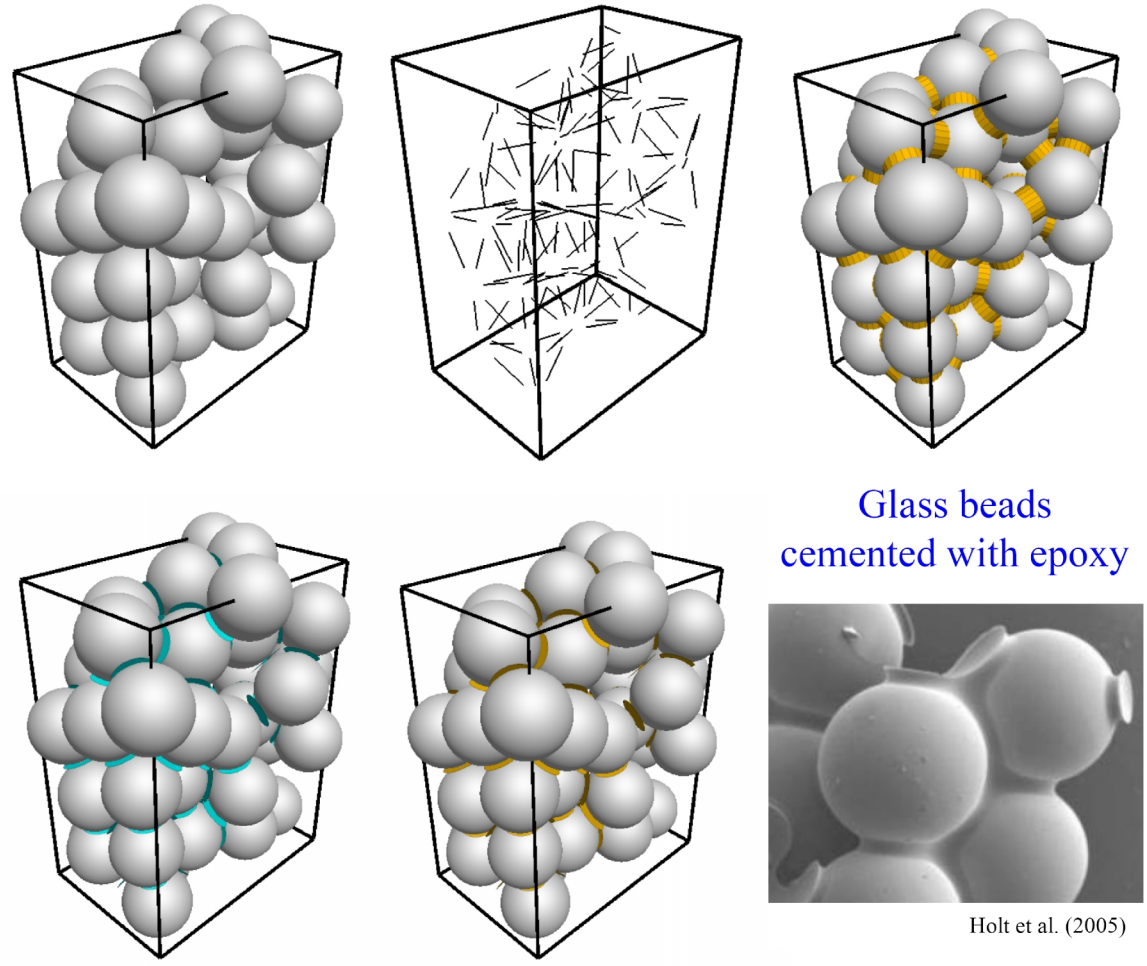

Figure 15 ***Microstructural plot sets for bonded materials with the same initial packing showing (clockwise from upper left): microstructural box and grains in the box (grey); contact-bonded material with contact bonds in the box; parallel-bonded material with parallel-bond cement (gold, 50% size) and parallel-bond interfaces (gold, 50% size); and flat-jointed material with flat-jointed interfaces (blue, 50% size).***

The faced grain plot set (geometry set name: **"faced grains"**) displays each grain of a flat-jointed material as a faced grain — only ball-shaped grains are displayed, clump-shaped grains are not supported (see Figure 16). To draw faced grains, the microstructure-tracking flag (C_{MS} in Table 5) must be set to true. The faced grains are created when the flat-joint model is installed at the ball-ball contacts of a packed ball assembly such that each face remains rigidly connected to its corresponding grain during subsequent motion. The faced grain is drawn as a spherical core with a skirted face at the associated notional surface of each flat-jointed contact. The core and skirted faces of each grain can be displayed by the geometry set plot item by specifying {ColorBy: Group}, {Slot: 1} and {Sets: faced grains},

with {Color-List:} used to turn each entity on/off and specify its color. For the 2D model, two geometry set plot items should be used. The first geometry set plot item turns on the entities 'core' and 'grain in skirt', with {Edges: Off}, {Polys: checked} and {Polys: Polygons: Outline: unchecked}. The second geometry set plot item turns on the entity 'skirted face', with {Edges: On} and {Polys: unchecked}. The visualization scheme for each entity is as follows.

a. **Core** (group 'core'). The core is drawn as a sphere with radius equal to the minimum of all facet radial distances. For the 2D model, the core is drawn as a circle.
b. **Skirted Face** (group 'skirted face', also 'grain in skirt' for the 2D model). The skirted face is drawn as a disk (line for the 2D model) surrounded by a skirt that extends toward the core center until it intersects the core surface.

The faced grain plot set displays only the faces joining grains with centers inside the microstructural box. This behavior can be modified by specifying the ID number of a seed grain (via **`msFG_seedID`**), and the number of grains connected directly to the seed grain (via **`msFG_seedNum`**) that should also be drawn.

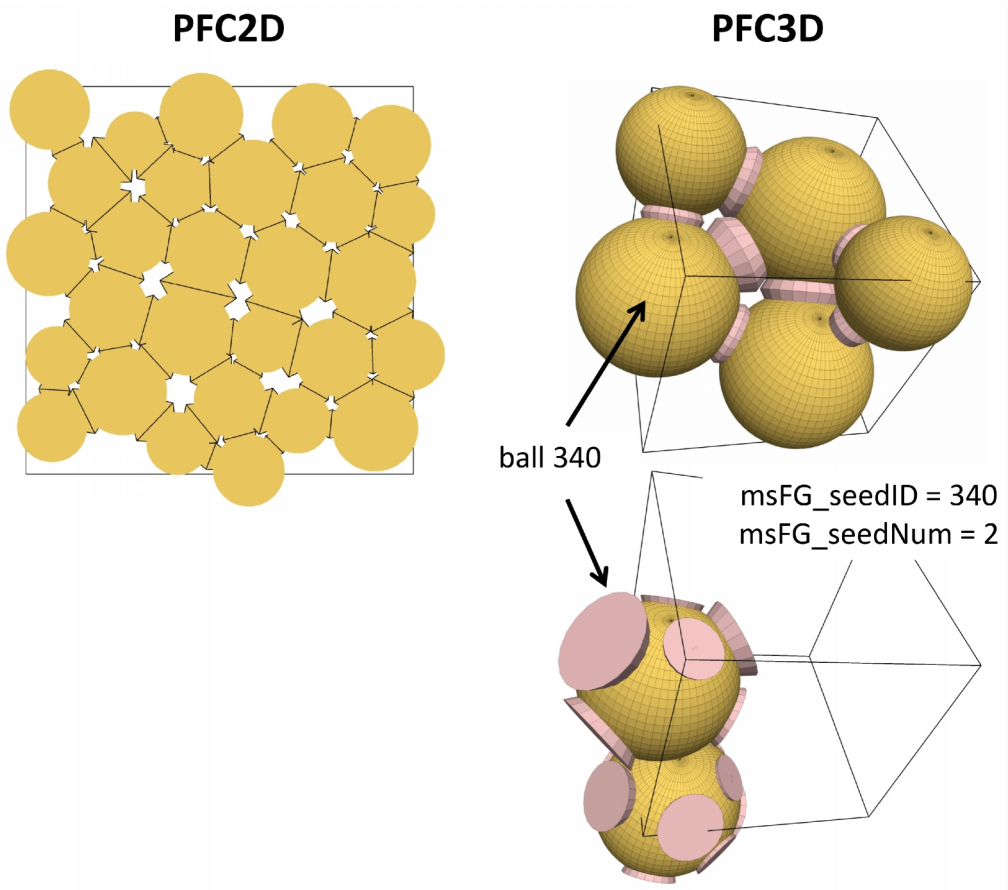

Figure 16 Faced grain plot set showing faced grains in the microstructural box (top) and connected to a seed grain (bottom).

Cracks. Damage in the bonded materials consists of bond breakages which we denote as cracks. Cracks are stored and visualized by the crack-monitoring package (see Section 3.4). The crack plot set (geometry set name: **"cracks"**) displays the cracks with thickness proportional to gap. The cracks and gap are taken from the crack-monitoring package. Cracks are drawn as thick disks for the 3D model, and thick lines of unit-thickness depth for the 2D model. The crack size is taken as the scale factor (**msCK_sfacSize**) times the size returned by the crack-monitoring package. The cracks can be displayed by the geometry set plot item by specifying {ColorBy: Group}, {Sets: cracks}, and {Polys: checked}, with {Colors:} used to turn each entity (crack type and failure mode) on/off and specify its color. Filtered cracks can be displayed by setting **msCK_ckFilter** to true. Ghost cracks, defined as the cracks for which the originating contact no longer exists, are not displayed. Only grain-grain cracks with both parent grains inside of the microstructural box are drawn.

Crack thickness is equal to the true gap, with the restriction that the thickness lies in the range $[t_{\min}, t_{\max}]$ where $t_{\min} = \alpha_1 \tilde{s}$, $t_{\max} = \alpha_2 \tilde{s}$, α_1 and α_2 (**msCK_sfacMinThick** and

msCK_sfacMaxThick) are scale factors, and $\tilde{s}$ is the average size of all displayed cracks. To draw all cracks with thickness equal to the positive gap (and minimum thickness for cracks with negative gap), set **sCK_sfacMaxThick = 1e20** (the default value). Examples of the 2D and 3D crack plot sets are shown in Figures 17 and 18.

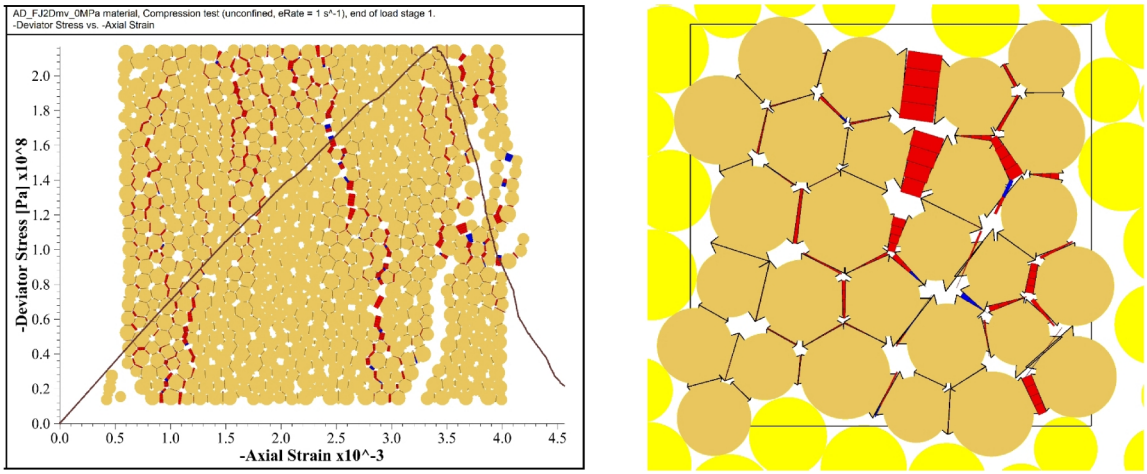

Figure 17 ***Crack and faced grain plot sets in 2D showing cracks, with crack thickness equal to gap, and cracks colored red/blue for tensile/shear failure. 2D flat-jointed material at end of UCS test as the specimen exhibits axial splitting.***

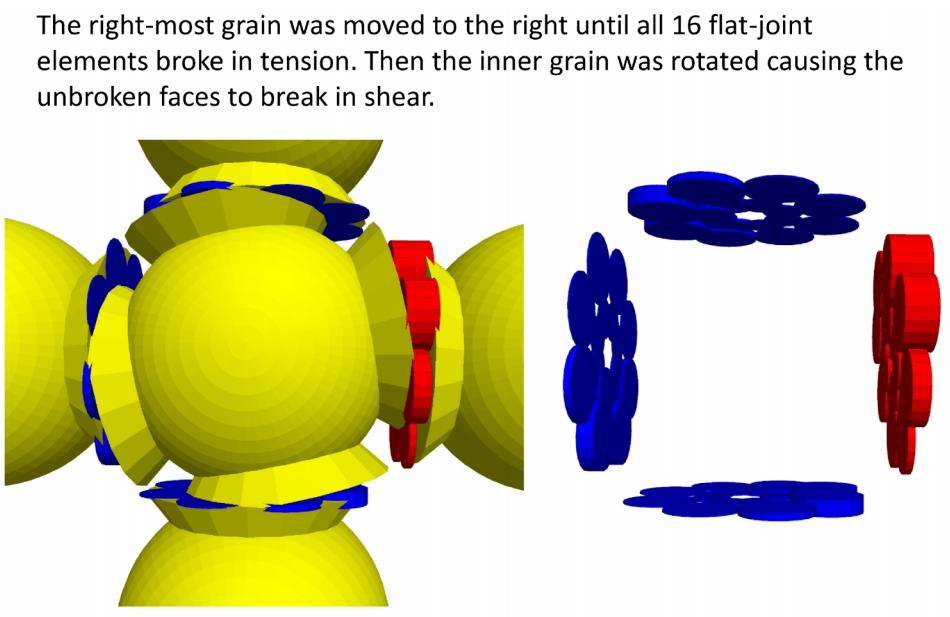

Figure 18 ***Crack and faced grain plot sets in 3D showing cracks, with crack thickness equal to gap, and cracks colored red/blue for tensile/shear failure.***

3.3 Force-Chain Fabric

The PFC material carries load via force chains that propagate from one grain to the next across grain-grain contacts. The force-chain fabric is depicted as a network of cylinders, with a cylinder at each contact. Force magnitude corresponds with cylinder thickness, and force direction corresponds with cylinder orientation. The force-chain fabric can be displayed as either bi-colored to denote compression and tension or scale-colored to denote magnitude (see Figure 19). Both displays are provided by the contact plot item. The bi-colored display is obtained by specifying: {Shape: Cylinder}, {Color By: Text Val: force chain}, {Color Opt: Named}, {Scale by Force: checked}, and {Directed: checked}. The scale-colored display is provided by specifying: {Shape: Cylinder}, {Color By: Vector Qty: force}, {Color Opt: Scaled}, {Scale by Force: checked}, and {Directed: checked}.

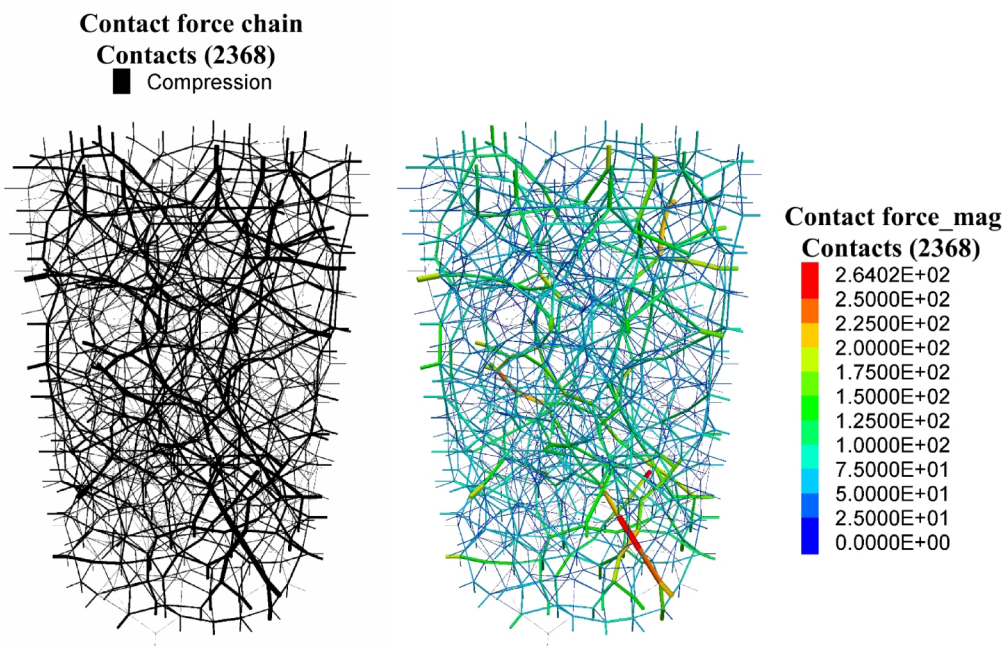

Figure 19 Force-chain fabric in the linear material packed at 150 kPa material pressure showing: bi-colored (left) and scale-colored (right) displays. The linear material cannot sustain tension, therefore the bi-colored display shows only compression.

3.4 Crack Monitoring

Damage in the bonded materials consists of bond breakages, which we denote as cracks. Each crack has: type (parallel bonded, contact bonded, flat jointed or smooth jointed); failure mode (tensile or shear); geometric information (size, position, normal direction and gap); step number at which it formed; and orphan indicator. The numbers of all cracks (partitioned by type and failure mode) are returned by the **`ck_nX`** functions. Crack data is stored as a Discrete Fracture Network (DFN). The

Fracture plot item supports visualization of the cracks.[29] Crack filtering occurs by calling the FISH function **ckFilter(** g **)**, which selects cracks with a gap less or greater than g (based on the value of **ckFilterOpen**). The **ckFilter** function can be redefined to provide a user-defined filtering criterion. The Fracture plot item displays cracks by specifying: {Shape: Fracture}, {Color By: Text Val: group (slot 1 or 2, for all or filtered cracks, respectively)}, and {Color Opt: Color-List: select on/off and color for each type and failure mode}. The size of the displayed cracks is scaled by the shrink factor in the Shape attribute of the Fracture plot item: {Shape: Shrink Factor}.

Geometric Information:

A crack is a disk for the 3D model and a linear segment of unit-thickness depth for the 2D model. A crack has a size (diameter for the 3D model and length for the 2D model), position, normal direction and gap.

- The size is set at creation and then frozen. The size for each type of crack is:
  - contact-bonded crack: two times the radius of the deformability method.
  - parallel-bonded crack: two times the parallel-bond radius.
  - flat-jointed crack: two times the element radius (which is the radius giving the same area as the element), or the element length (for the 2D model).
  - smooth-jointed crack: two times the smooth-joint radius.
- The position, normal direction and gap are updated to correspond with material motion subsequent to bond breakage (see **ckForceUpdate**). If the originating contact exists, then these quantities are obtained from the contact and its associated contact model as described below. If the originating contact no longer exists, then these quantities are set equal to the contact-plane location, contact-plane normal direction and contact gap, respectively, that would be assigned to a contact between the two parent pieces.[30] However, if at least one of the parent pieces no longer exists, then these quantities are frozen at their last updated values, and such cracks are called orphans. The crack position is given by

$$\mathbf{x} = \begin{cases} \mathbf{x}^{(e)}, & \text{flat-jointed crack} \\ \mathbf{x}_\mathbf{c}, & \text{otherwise} \end{cases} \tag{4}$$

where $\mathbf{x}^{(e)}$ is the centroid location of element (e), and $\mathbf{x}_\mathbf{c}$ is the contact-plane location. The crack normal direction is given by

[29] The cracks displayed by the Fracture plot item have zero thickness. The microstructural plot set "cracks" displays cracks with thickness proportional to gap.

[30] The three geometric quantities are given by Eq. (2) in Itasca (2018, PFC: PFC Model Objects: Contacts and Contact Models: Contact Resolution).

$$\hat{\mathbf{n}} = \begin{cases} \hat{\mathbf{n}}_{\mathbf{j}}, & \text{smooth-jointed crack} \\ \hat{\mathbf{n}}_{\mathbf{c}}, & \text{otherwise} \end{cases} \tag{5}$$

where $\hat{\mathbf{n}}_{\mathbf{j}}$ is the joint normal direction, and $\hat{\mathbf{n}}_{\mathbf{c}}$ is the contact-plane normal direction. The crack gap is given by

$$g = \begin{cases} g_s = g_c - g_r, & \text{contact- or parallel-bonded crack} \\ g^{(e)}, & \text{flat-jointed crack} \\ g_j, & \text{smooth-jointed crack} \end{cases} \tag{6}$$

where g_s is the surface gap, g_c is the contact gap, g_r is the reference gap, $g^{(e)}$ is the gap at the centroid of element (e), and g_j is the joint gap.

Global Functions:

- **`ckInit, ckOn, ckOff, ckForceUpdate, ckListData, ck_nOrphans, ck_nFiltered`**. The crack-monitoring package is initialized and turned on by calling **`ckInit`**. If the package is reinitialized, then crack data is reset. The package is activated by **`ckOn`**, and deactivated by **`ckOff`**. Cracks are only monitored when the package is on. The crack data can be listed to the screen by **`ckListData`**.

Global Variables:

- **`ck_nAll`**, **`ck_n{CB,PB,FJ,SJ}{t,s}`** : crack counts (used with history logic to monitor cracking during a simulation)
- **`ckUpdateRate`** : crack geometry update rate (number of cycles)
- **`ckFilterGap`** : display cracks with gap less (**`ckFilterOpen = 0`**) or greater (**`ckFilterOpen # 0`**) than this value (used by **`ckFilter`**)
- **`ckFilterOpen`** : see **`ckFilterGap`**

Crack Data (stored for each crack, which is a DFN fracture):

- The size, position and normal direction are stored as DFN data.
- **group (slot 1)** : name indicating type & failure mode (**`{CB,PB,FJ,SJ}-{ten,shear}Fail`**) of all cracks
  group (slot 2) : name indicating type, failure mode and gap-based filtering criterion (**`{CB,PB,FJ,SJ}-{ten,shear}Fail(gap < [ckFilterGap])`**) of filtered cracks
- **extra 1** : originating contact
  extra 2 : originating element (for flat-jointed cracks only)

extra 3 : parent piece-1 (ball or pebble)
extra 4 : parent piece-2 (ball, pebble or facet)
extra 5 : gap
extra 6 : step number at which the crack formed
extra 7 : orphan indicator (1: orphaned crack, 0: not an orphaned crack)

4.0 MATERIAL GENESIS

Material behavior is embodied in the contact model at the grain-grain contacts. The material-genesis procedure creates the following PFC materials: linear, contact-bonded, parallel-bonded, flat-jointed and user-defined.[31] There is a **`MatGen`** project for each material type, and these projects are in directories: **`MatGen-X`**, where **`X = {Linear, ContactBonded, ParallelBonded, FlatJointed, Hill}`**. The materials consist of a homogeneous, isotropic and well-connected grain assembly with a specified non-zero material pressure. Material genesis occurs within a material vessel that may be either a physical vessel or a periodic space. Materials formed in a physical vessel may be removed from the vessel for subsequent boundary-value modeling, while materials formed in periodic space may also have an installed stress state and are converted into a periodic brick, and then assembled into a specimen for subsequent boundary-value modeling.[32] The boundary-value modeling may involve trimming the material into a desired shape and applying boundary conditions. The material vessels are described in the first subsection. The material-genesis procedure is described in the second subsection.

4.1 Material Vessels

Material genesis occurs within a material vessel that may be either a physical vessel or a periodic space. The physical vessels include polyaxial, cylindrical and spherical cells (see Figure 20). A polyaxial cell consists of planar walls that form a rectangular cuboid (for which each pair of adjacent faces meets in a right angle). A cylindrical cell consists of two planar walls and a cylinder wall. A spherical cell consists of a sphere wall. Walls of the physical vessels are expanded to prevent grains from escaping if the walls are moved outwards during subsequent compression testing — the wall-wall overlap is ignored, because walls interact only with grains. For materials formed in periodic space, the periodic cell is a rectangular cuboid (see Figure 21). A stress state that has no shear components and does not vary with position can be installed into the finalized periodic assembly (after bonding) by deforming the periodic space ($C_s = 1$) using a subset of the more general scheme of Itasca (2008a&b).[33] Three spherical measurement regions are placed symmetrically along the axis of the largest vessel dimension (with a spanning length of α_l times the largest vessel dimension, and with a diameter of α_d times the smallest vessel dimension). For materials formed in a physical vessel, the linear contact model is installed at the grain-wall contacts. The walls are frictionless, and grain-wall contact stiffness is set based on a specified contact deformability (E^* of the **deformability** method of the linear model). The material vessel parameters are listed in Table 6.

---

[31] The material-genesis procedure in the PFC 6.0 FISHTank creates a homogeneous material and does not include the material and refinement regions of the PFC 4.0 FISHTank.

[32] The brick is assembled into a specimen by calling **`Assemble.p{2,3}dvr`** from the **`MatGen`** project.

[33] In the PFC 4.0 manuals in Section 3.9 Stress-Installation Procedure, in the *FISH in PFC3D/2D* volumes. The deformation occurs such that the difference between the current and target stresses is reduced by approximately one half during each step.

Table 6 Material-Vessel Parameters

Parameter, FISH	Type	Range	Default	Description
Material-vessel properties (including current vessel dimensions) are listed via **`@mvListProps`**.				
T_v, **`mv_type`**	INT	$\{0,1\}$	0	vessel-type code $\begin{cases} 0, & \text{physical} \\ 1, & \text{periodic} \end{cases}$
S_v, **`mv_shape`**	INT	$\{0,1,2\}$	0	vessel-shape code $\begin{cases} 0, & \text{rectangular cuboid} \\ 1, & \text{cylinder} \\ 2, & \text{sphere} \end{cases}$ (2D model: $S_v \equiv 0$)
$\{H,W,D\}$, **`mv_{H,W,D}`**	FLT	$(0.0,\infty)$	NA	height, width and depth (sphere diameter is H; 2D model: $D \equiv 1$, see Figure 2)
C_s, **`mv_Sinstall`**	INT	$\{0,1\}$	0	stress-installation code $\begin{cases} 0, & \text{do not install stress} \\ 1, & \text{install stress} \end{cases}$
$\{\sigma_{xx},\sigma_{yy},\sigma_{zz}\}$, **`mv_S{x,y,z}`**	FLT	$(-\infty,\infty)$	NA	installation stresses $(T_v = 1 \text{ and } C_s = 1)$
ε_s, **`mv_Stol`**	FLT	$(0.0,\infty)$	1×10^{-2}	stress tolerance $\left(\left\|\frac{\sigma_{ii} - \sigma_{ii}^t}{\sigma_{ii}^t}\right\| \le \varepsilon_s\right),\ i = 1,2,3$ where σ_{ii} is current stress
E, **`mv_Semod`**	FLT	$(0.0,\infty)$	NA	ensemble modulus $\left(\dot{\varepsilon}_{ii} = \frac{1}{2E\Delta t}\left(\sigma_{ii} - \sigma_{ii}^t\right)\right)$
ε_{lim}, **`mv_SARatLimit`**	FLT	$(0.0,\infty)$	1×10^{-5}	equilibrium-ratio limit (parameter of **`ft_eq`**)
α, **`mv_expandFac`**	FLT	$[1.0,\infty)$	1.2	expansion factor of physical vessel
$\{\alpha_l,\alpha_d\}$, **`mv_inset{L,D}Fac`**	FLT	$(0.0,1.0]$	{0.8, 0.8}	inset factors of measurement regions
E_v^*, **`mv_emod`**	FLT	$(0.0,\infty)$	NA	effective modulus of physical vessel

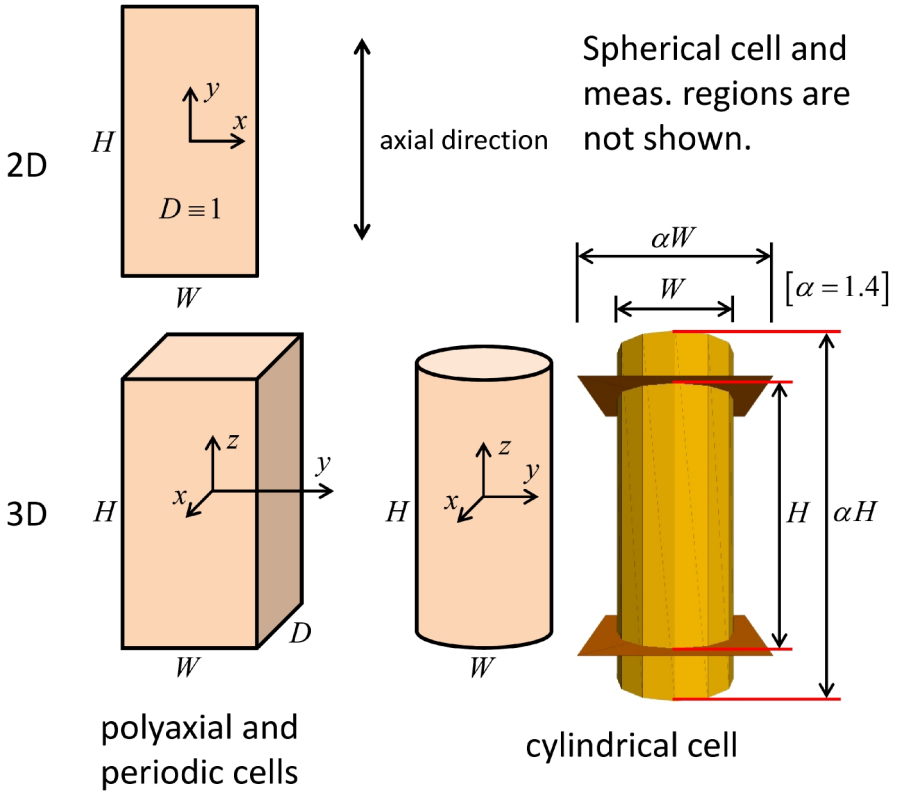

Figure 20 Material vessels with global coordinate system centered in each cell and associated axial direction.

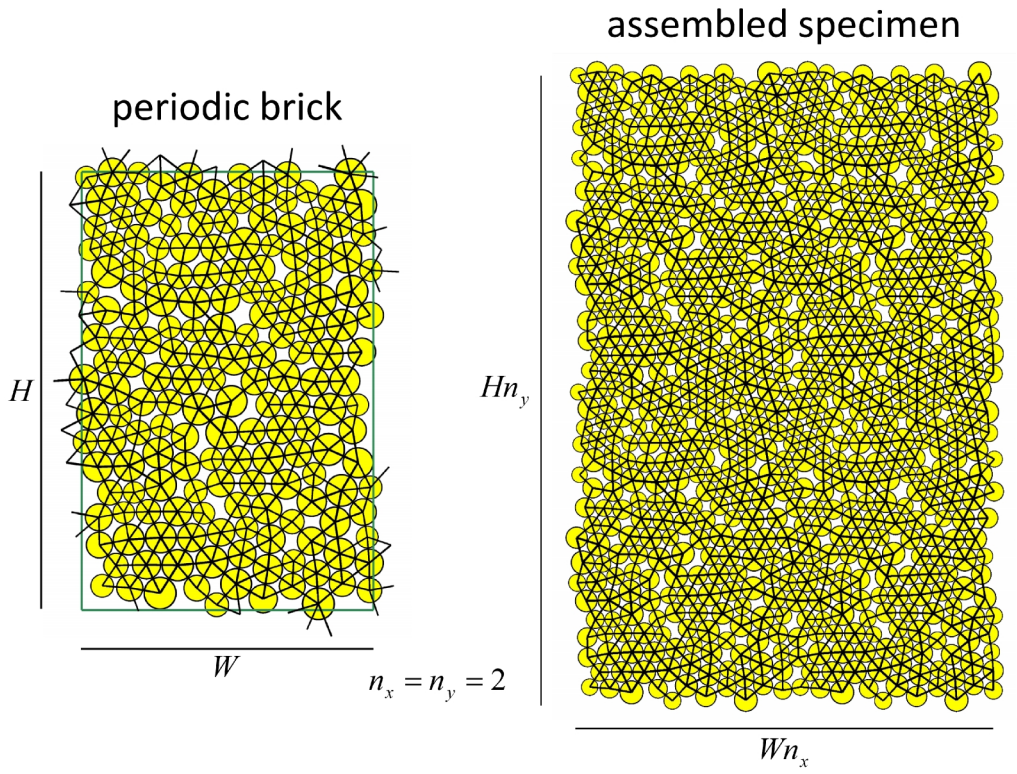

Figure 21 Packed particle ensemble in periodic material vessel (left) and assembled into a larger geometric shape (right), with contacts shown as black lines.

4.2 Material-Genesis Procedure

The material-genesis procedure occurs within the material vessel and produces a specimen consisting of a homogeneous, isotropic and well-connected grain assembly with a specified non-zero material pressure. The material-genesis procedure consists of a packing phase followed by a finalization phase. During the packing phase, the grain assembly is subjected to a specified packing procedure. During the finalization phase, the final material properties are assigned to the grain-grain contacts, and additional material properties are specified that will be assigned to new contacts that may form during subsequent motion. The two phases are described in the following two subsections.

4.2.1 Packing Phase

During the packing phase, the grain assembly is subjected to a specified packing procedure during which the effective behavior at all grain-grain contacts is that of either the linear contact model or a user-defined contact model. For the linear model, the properties are deformability (**`lnm_emod`** and **`lnm_krat`**); for the user-defined model, the properties are specified in the redefined **`ft_setMatBehavior`** FISH function. The friction coefficient is a packing parameter (either zero or μ_{CA} in Table 7).

The packing procedures include boundary contraction and grain scaling. Boundary contraction is available only for the physical material vessel, while grain scaling is available for both the physical and periodic material vessels. The boundary-contraction procedure produces a dense or loose packing of a granular material, while the grain-scaling procedure produces a dense packing of a granular material that will subsequently become a bonded material during the material-finalization phase. Both procedures generate a cloud of grains, and then allow them to rearrange into a packed state under conditions of zero friction. The desired material pressure is obtained differently for each procedure. For the boundary-contraction procedure, confinement is applied by moving the vessel walls under control of the servomechanism described in Section 5.3, whereas for the grain-scaling procedure, the grain sizes are scaled iteratively to modify the mean stress of the assembly. For the boundary-contraction procedure, the material friction coefficient is chosen during confinement application to achieve a dense or loose packing, whereas for the grain-scaling procedure, the material friction coefficient remains equal to zero throughout the entire packing process to achieve a dense packing. The packing parameters are listed in Table 7. A series of material instances can be created with the same statistical properties but different packing arrangements by varying the seed of the random-number generator.

Table 7 Packing Parameters

Parameter	Type	Range	Default	Description
S_{RN} , **pk_seed**	INT	$S_{RN} \geq 10{,}000$	$10,000$	seed of random-number generator (affects packing)
P_m , **pk_Pm**	FLT	$(0.0, \infty)$	NA	material pressure
ε_P , **pk_PTol**	FLT	$(0.0, \infty)$	1×10^{-2}	pressure tolerance $\left(\frac{\lvert P - P_m \rvert}{P_m} \leq \varepsilon_P \right)$ where P is current pressure
$\varepsilon_{\lim}$, **pk_ARatLimit**	FLT	$(0.0, \infty)$	8×10^{-3}	equilibrium-ratio limit (parameter of **ft_eq**)
$n_{\lim}$, **pk_stepLimit**	INT	$[1, \infty)$	2×10^{6}	step limit (parameter of **ft_eq**)
C_p , **pk_procCode**	INT	$\{0,1\}$	0	packing-procedure code $\begin{cases} 0, & \text{boundary contraction} \\ 1, & \text{grain scaling} \end{cases}$
n_c , **pk_nc**	FLT	$(0.0, 1.0)$	$\begin{cases} \begin{cases} 0.58, & \text{3D} \\ 0.25, & \text{2D} \end{cases}, & C_p = 0 \\ \begin{cases} 0.35, & \text{3D} \\ 0.08, & \text{2D} \end{cases}, & C_p = 1 \end{cases}$	grain-cloud porosity

Boundary-contraction group ($C_p = 0$):				
μ_{CA} , **pk_fricCA**	FLT	$[0.0, \infty)$	0.0	material friction coefficient during confinement application
v_{lim} , **pk_vLimit**	FLT	$(0.0, \infty)$	NA	servo velocity limit (see Table 9)

Static-equilibrium is determined by successful return from the **ft_eq** FISH function:

- **ft_eq(** ε_{lim} **,** n_{lim} **)** cycles the model until a state of static equilibrium is obtained. Cycling continues until either the mechanical ratio-average ($\varepsilon_{\text{arat}}$) falls below the equilibrium-ratio limit $(\varepsilon_{\text{lim}})$:

$$\varepsilon_{\text{arat}} \le \varepsilon_{\text{lim}} \quad [\text{command: model solve ratio-average } \varepsilon_{\text{lim}}]$$

or the number of steps (n_s) exceeds the step limit (n_{lim}):

$$n_s > n_{\text{lim}} \quad [\text{command: model solve cycles } n_{\text{lim}}].$$

The ratio-average and ratio-maximum are defined as

$$\varepsilon_{\text{arat}} = \frac{\text{avg}\{\|\mathbf{F_{ub}}\|\}}{\text{avg}\{F_{\text{int}}\}} = \frac{\sum_{n_g} \|\mathbf{F_c} + \mathbf{F_a} + \mathbf{F_b}\| \Big/ n_g}{\sum_{n_g} \left(\|\mathbf{F_c}\| + \|\mathbf{F_a}\| + \|\mathbf{F_b}\|\right) \Big/ n_g}$$

$$\varepsilon_{\text{mrat}} = \frac{\max\{\|\mathbf{F_{ub}}\|\}}{\text{avg}\{F_{\text{int}}\}} = \frac{\max \sum_{n_g} \|\mathbf{F_c} + \mathbf{F_a} + \mathbf{F_b}\|}{\sum_{n_g} \left(\|\mathbf{F_c}\| + \|\mathbf{F_a}\| + \|\mathbf{F_b}\|\right) \Big/ n_g}$$

The ratio-average is the average (over all grains) unbalanced force magnitude divided by the average (over all grains) force intensity, while the ratio-maximum is the maximum (over all grains) unbalanced force magnitude divided by the average (over all grains) force intensity. The unbalanced force is the vector sum of all forces acting on the grain (contact, applied and body), and the force intensity is the sum of the force magnitudes. In the above expressions, vector magnitude is defined by $\|\mathbf{v}\| = \sqrt{v_x^2 + v_y^2 + v_z^2}$, and only free translational degrees-of-freedom are used in the computations.

The boundary-contraction procedure is adapted from McDowell et al. (2006) and consists of the following three steps (see Figure 22).

1. Generate a cloud of grains with porosity of n_c. This porosity does not account for overlaps: $n_c = \left(V_v - V_g\right)/V_g$, where V_v is the volume of the material vessel and V_g is the total volume of grains. The grains are drawn from the specified size distribution, and then placed at arbitrarily chosen positions that lie fully within the material vessel such that there may be large grain-grain overlaps. Typically, n_c is chosen equal to n_l, where n_l corresponds with the loose state for which grains are just in contact at zero mean stress. For a linear material of equal-sized spheres, $n_l = 0.58$. For a linear material of equal-sized disks, $n_l = 0.25$.
2. Set the material friction coefficient to zero, and then allow the grains to rearrange until either the mean stress is near zero (within 0.1% of P_m) or static-equilibrium is obtained.[34] This step eliminates the large overlaps and should provide an isotropic state.
3. Set the material friction coefficient to μ_{CA}, and then apply confinement of P_m . The confinement is applied by moving the vessel walls under control of the servomechanism until the wall pressures are within the specified pressure tolerance of the material pressure and static-equilibrium has been obtained. Setting $\mu_{CA} = 0$ gives the densest packing, and progressively looser packings are obtained by increasing μ_{CA}.

[34] During the first set of cycles, the model is calmed (by setting all grain translational and rotational velocities to zero) every five steps, and the calming continues until the maximum overlap ratio (defined at the active contacts as the contact gap divided by the piece diameter) is small (less than **`_pkORmaxLimit`**, which defaults to 0.25). The calming process prevents most grains from passing through the walls of the material vessel; those grains with centers lying outside of the material vessel at the end of step 2 are deleted, and for clumped materials, those pebbles with centers lying outside of the material vessel are also deleted.

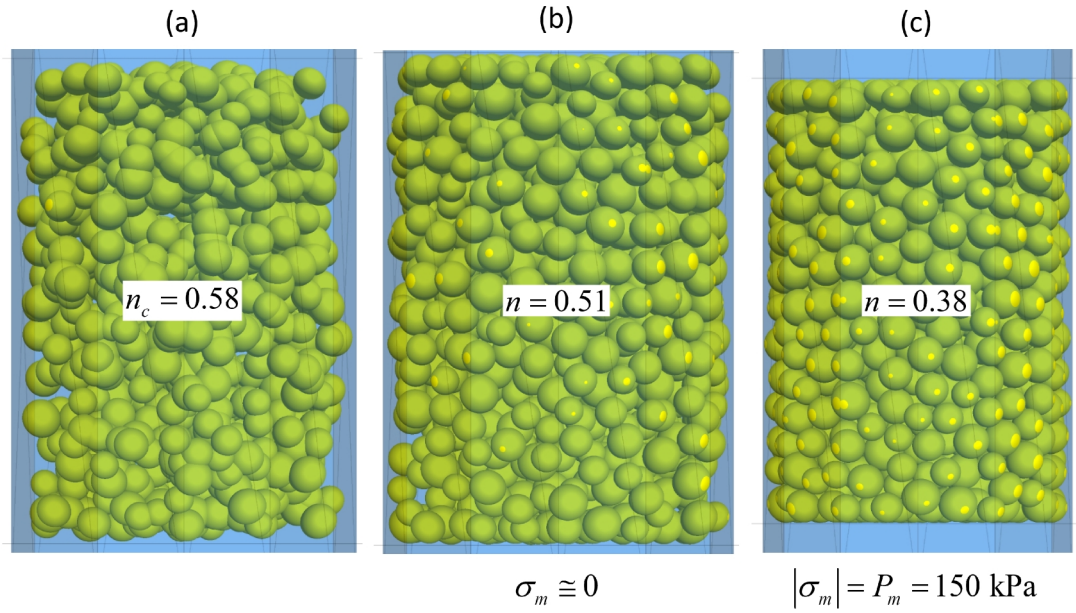

Figure 22 Boundary-contraction packing procedure: (a) initial grain cloud at end of step 1, (b) relaxed grain cloud at end of step 2, and (c) compacted granular assembly at end of step 3. The images show the AG_Linear material of the linear material example.

The grain-scaling procedure is similar to what is referred to as the material-genesis procedure in Potyondy and Cundall (2004) and Itasca (2008a&b, Section 3.6.2 Material-Genesis Procedure, in *FISH* in *PFC3D*/*PFC2D* volumes) and consists of the following three steps (see Figure 23).

1. Generate a cloud of grains with porosity of n_c. This porosity does not account for overlaps: $n_c = \left(V_v - V_g\right)/V_g$, where V_v is the volume of the material vessel and V_g is the total volume of grains. The grains are drawn from the specified size distribution, and then placed at arbitrarily chosen positions that lie fully within the material vessel such that there may be large grain-grain overlaps. Typically, n_c is chosen equal to n_d, where n_d corresponds with the dense state for which grains are well packed and in good contact with one another at a large mean stress but with relatively small overlaps. For a linear material of equal-sized spheres, $n_d = 0.35$. For a linear material of equal-sized disks, $n_d = 0.08$.
2. Set the material friction coefficient to zero, and then allow the grains to rearrange until either the mean stress is near zero (within 0.1% of P_m) or static-equilibrium is obtained (see footnote 34). This step eliminates the large overlaps and should provide an isotropic and close-packed state.
3. Scale the grain size iteratively to modify the mean stress of the assembly until the mean stress is within the specified pressure tolerance of the material pressure and static-

equilibrium has been obtained. The grain-scaling procedure is described in Itasca (2008a&b, Section 3.10.3 Isotropic Stress Installation Procedure, in *FISH* in *PFC3D*/*PFC2D* volumes). For a bonded material, the material pressure is typically set to a low value relative to the material strength.

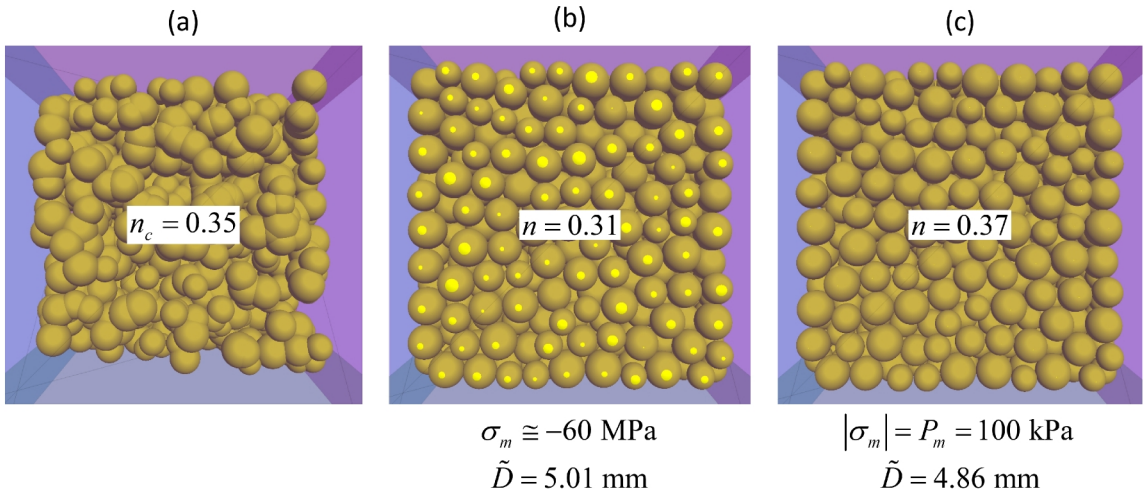

Figure 23 ***Grain-scaling packing procedure: (a) initial grain cloud at end of step 1, (b) relaxed grain cloud at end of step 2, and (c) compacted granular assembly at end of step 3. The images show the SS_ContactBonded material of the contact-bonded material example.***

4.2.2 Finalization Phase

During the finalization phase, the final material properties are assigned to the grain-grain contacts, and additional material properties are specified that will be assigned to new contacts that may form during subsequent motion. The first step of the finalization phase occurs only for the bonded materials. We ensure the existence of contacts between all grains with a gap less than or equal to the installation gap by specifying the installation gap as the proximity in the Contact Model Assignment Table and executing the CLEAN command; this operation may create new grain-grain contacts in the grain assembly. The grain connectivity is controlled by the material pressure and the installation gap, with the installation gap being of primary importance (see Figure 24). The next step of the material-finalization phase differs for each material as follows.

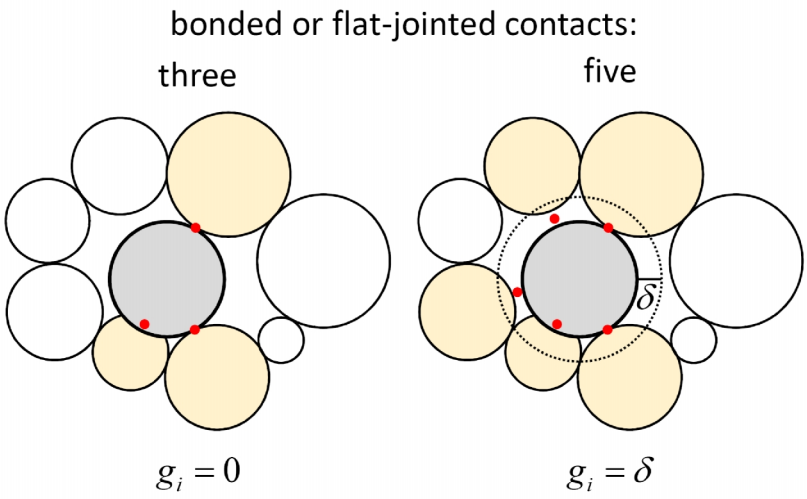

Figure 24 Grain assembly at end of packing phase with the bonded or flat-jointed contacts of a typical grain when the installation gap is zero (left) and greater than zero (right). Increasing the installation gap increases the grain connectivity.

- For a **linear material**, the linear material properties (from Table 2) are assigned to all grain-grain contacts. New grain-grain contacts that may form during subsequent motion are assigned the linear model with properties derived from the linear material properties.
- For a **contact-bonded material**, the contact-bonded material properties (from Table 3) are assigned to all grain-grain contacts, but only those grain-grain contacts with a gap less than or equal to the installation gap are bonded. New grain-grain contacts that may form during subsequent motion are assigned the linear contact bond model with properties derived from the linear material group of the contact-bonded material properties, and the new contacts are unbonded.
- For a **parallel-bonded material**, the parallel-bonded material properties (from Table 4) are assigned to all grain-grain contacts, but only those grain-grain contacts with a gap less than or equal to the installation gap are bonded. New grain-grain contacts that may form during subsequent motion are assigned the linear parallel bond model with properties derived from the linear material group of the parallel-bonded material properties, and the new contacts are unbonded.
- For a **flat-jointed material**, the flat-joint contact model is installed at all grain-grain contacts with a gap less than or equal to the installation gap, and the flat-jointed material properties (from Table 5) are assigned to these flat-jointed contacts. The remaining grain-grain contacts as well as new grain-grain contacts that may form during subsequent motion are assigned the linear model with properties derived from the linear material group of the flat-jointed material properties.

- For a **user-defined material**, the user-defined material properties are assigned to all grain-grain contacts. New grain-grain contacts that may form during subsequent motion are assigned the user-defined model with properties derived from the user-defined material properties.

For the bonded materials, the final material properties are set to establish reference surfaces that do not overlap (see Figure 25); therefore, there are no forces or moments in the bonded material. For the bonded materials, the grain-vessel interface is smoothed (see Figure 26). The smoothing operation consists of setting the reference gap equal to the contact gap for all grain-wall contacts with a negative contact gap (thereby establishing reference surfaces that are just touching and effectively removing the overlap). After the smoothing operation and the assignment of the final material properties, there are no forces at the grain-wall interface and no forces or moments in the bonded material. Subsequent compression testing will proceed as expected, because the specimen will become loaded during the seating phase as the vessel walls move inward. New grain-wall contacts will be created naturally, because only the grain-wall contacts protruding from the vessel at the time of smoothing were affected by the smoothing operation.

The system is brought to static equilibrium while keeping the walls fixed. The specimen remains within the material vessel, and the model state is saved. This model state can be restored for subsequent materials testing. If a bonded material is being created, then the specimen is removed from the material vessel and brought to static equilibrium, and the model state is saved. This model state can be restored for subsequent boundary-value simulation.

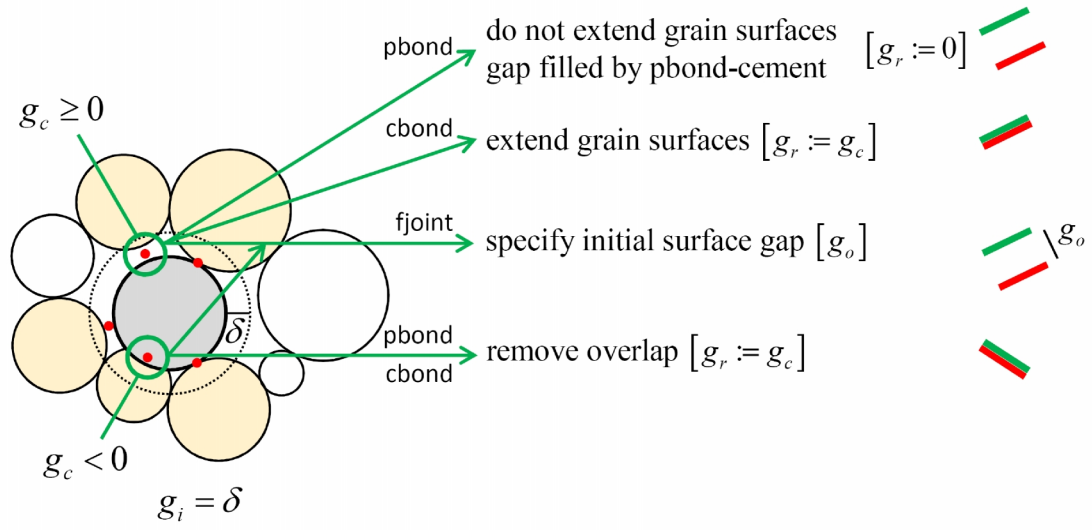

Figure 25 Setting final material properties of bonded materials to establish reference surfaces that do not overlap (contact-bonded, parallel-bonded and flat-jointed materials denoted by cbond, pbond and fjoint, respectively).

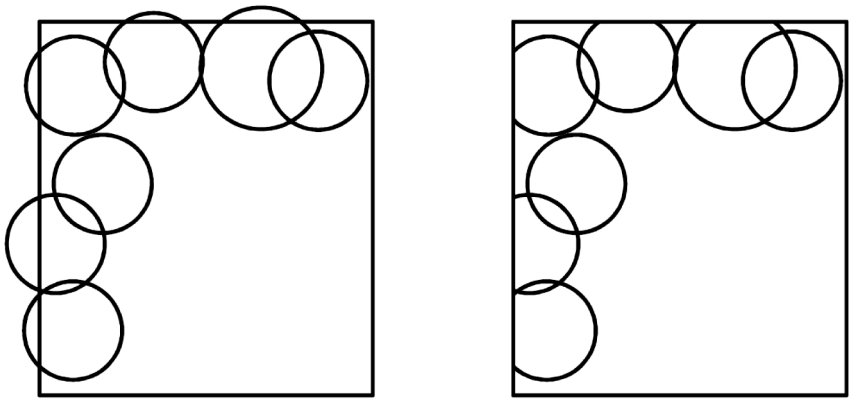

Figure 26 ***The effective grain-vessel interface before (left) and after (right) the smoothing operation, which effectively cuts off the part of each ball or pebble that protrudes from the material vessel.***

5.0 LABORATORY-TESTING PROCEDURES

The following standard rock-mechanics laboratory tests are supported: compression (confined, unconfined and uniaxial strain), diametral-compression, direct tension and fracture toughness (see Figure 27). The tests are performed upon materials that were created within the physical material vessel; however, the diametral-compression test can be performed upon any specimen that is centered at the origin. The loading axis corresponds with the axial direction shown in Figure 20. The specimen is loaded by walls in the compression and diametral-compression tests, and by surface grains in the direct-tension and fracture-toughness tests (after having been removed from the material vessel and allowed to relax). In the compression tests, the specimen is loaded in either a polyaxial or cylindrical cell in which the axial walls act as loading platens. For the confined test, the velocities of the radial walls are controlled by a servomechanism to maintain a constant confining pressure (P_c); for the unconfined test, the radial walls do not contact the specimen; and for the uniaxial-strain test, the radial walls are kept motionless. In the diametral-compression test, the specimen (typically of a cylindrical or spherical shape) is loaded by the axial walls. In the direct-tension and fracture-toughness tests, the velocities of selected surface grains are fixed in the axial direction, thereby pulling apart the opposing specimen surfaces.

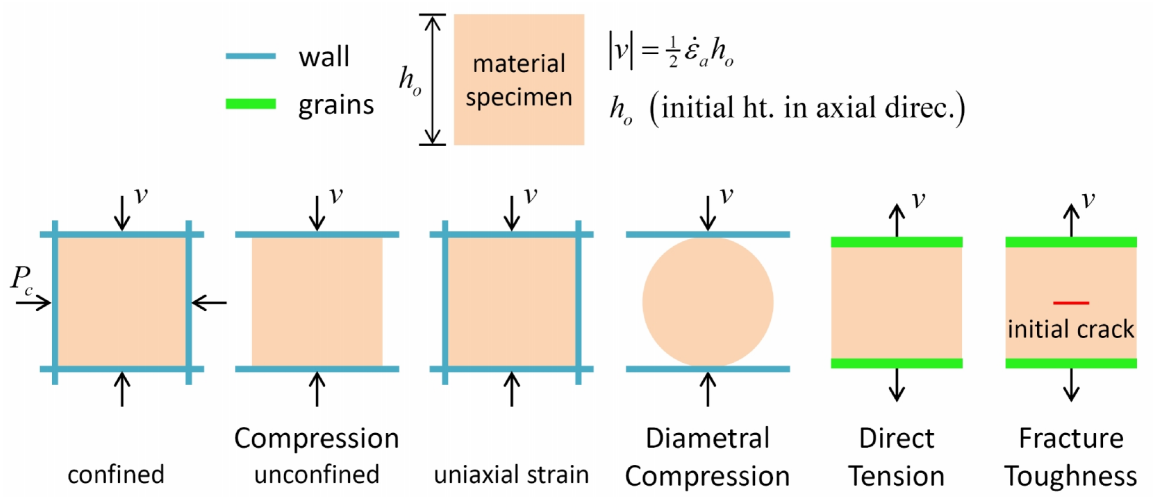

Figure 27 Loading conditions of laboratory-testing procedures.

The techniques used to measure stress, strain and porosity of the specimen within the material vessel are described in the first subsection. The measurement of material deformability is discussed in the second subsection. The servomechanism that controls wall velocities of the polyaxial, cylindrical and spherical cells is described in the third subsection. A discussion of how loading rate affects material response is given in the fourth subsection. The laboratory-test procedures are described in the remaining subsections.

5.1 Stress, Strain and Porosity in the Material

Stress and strain of the specimen within the material vessel is measured in three different ways via measurement regions, walls and gauge grains. The measurement-based quantities are taken as the average values from three spherical measurement regions that are placed symmetrically along the axis of the largest vessel dimension. The measurement logic is described in Itasca (2018)[35]. The wall-based quantities provide stress as wall force divided by cross-sectional area of specimen side (using either the current or initial vessel dimensions), and strain based on the change of distance between opposing walls. The gauge-based quantities are obtained from gauge grains that mimic LVDTs touching the specimen surface. Each gauge grain is the ball or clump that lies closest to the center of the corresponding specimen surface. The gauge-based quantities provide strain based on the change of distance between opposing gauge grains. Damage formation in a bonded material may perturb the gauge grains, and thus, wall-based quantities provide a more uniform averaged response over the entire specimen surface.

Porosity of the specimen within the material vessel is measured in two different ways via the above measurement regions and walls. The measurement-based porosity (n) accounts for grain-grain overlap via the procedure described in Itasca (2018)[36]. The wall-based porosity (n_w) does not account for overlaps: $n_w = \left(V_v - V_g\right)/V_g$, where V_v is the current volume of the material vessel and V_g is the total volume of grains.

We denote stress and strain by

$$\begin{aligned} &\text{stress:} \quad \left\{\sigma_{xx}, \sigma_{yy}, \sigma_{zz}, \sigma_{xy}, \sigma_{xz}, \sigma_{yz}\right\} \\ &\text{strain:} \quad \left\{\varepsilon_{xx}, \varepsilon_{yy}, \varepsilon_{zz}, \varepsilon_{xy}, \varepsilon_{xz}, \varepsilon_{yz}\right\} \end{aligned} \tag{7}$$

where $\sigma_{ii} > 0$ is tension and $\varepsilon_{ii} > 0$ is extension. For the 2D model, the out-of-plane stress and strain components are equal to zero so that stress is $\left\{\sigma_{xx}, \sigma_{yy}, \sigma_{xy}\right\}$ and strain is $\left\{\varepsilon_{xx}, \varepsilon_{yy}, \varepsilon_{xy}\right\}$. An axial direction is associated with each material vessel: the axial direction of the polyaxial and cylindrical cells for the 3D model corresponds with the z-direction, while the axial direction of the polyaxial cell for the 2D model corresponds with the y-direction (see Figure 20). The radial direction is perpendicular to the axial direction. We define the following stress and strain quantities.

[35] In documentation set at Program Guide: Common Model Objects: Measure.
[36] In documentation set at Program Guide: Common Model Objects: Measure: Measured Quantities: Porosity.

- Axial and radial stress and strain (3D model):

$$\sigma_a = \sigma_{zz}, \quad \sigma_r = \frac{1}{2}\left(\sigma_{xx} + \sigma_{yy}\right)$$
$$\varepsilon_a = \varepsilon_{zz}, \quad \varepsilon_r = \frac{1}{2}\left(\varepsilon_{xx} + \varepsilon_{yy}\right) \tag{8}$$

- Axial and radial stress and strain (2D model, $\varepsilon_{zz} \equiv \sigma_{zz} \equiv 0$):

$$\sigma_a = \sigma_{yy}, \quad \sigma_r = \sigma_{xx}$$
$$\varepsilon_a = \varepsilon_{yy}, \quad \varepsilon_r = \varepsilon_{xx} \tag{9}$$

- Deviator stress and strain:[37]

$$\sigma_d = \sigma_a - \sigma_r, \quad \varepsilon_d = \varepsilon_a - \varepsilon_r \tag{10}$$

- Mean stress and volumetric strain (3D model):

$$\sigma_m = \frac{1}{3}\left(\sigma_{xx} + \sigma_{yy} + \sigma_{zz}\right) = \frac{1}{3}\left(\sigma_a + 2\sigma_r\right), \quad \varepsilon_v = \varepsilon_{xx} + \varepsilon_{yy} + \varepsilon_{zz} = \varepsilon_a + 2\varepsilon_r \tag{11}$$

- Mean stress[38] and volumetric strain (2D model, $\varepsilon_{zz} \equiv 0$):

$$\sigma_m = \frac{1}{2}\left(\sigma_{xx} + \sigma_{yy}\right) = \frac{1}{2}\left(\sigma_a + \sigma_r\right), \quad \varepsilon_v = \varepsilon_{xx} + \varepsilon_{yy} + \varepsilon_{zz} = \varepsilon_a + \varepsilon_r \tag{12}$$

The material-vessel stress, strain and porosity quantities are listed in Table 8. The FISH variables for the measurement-based quantities are denoted by **`mv_mX`**, while the wall- and gauge-based quantities are denoted by **`mv_wX`** and **`mv_gX`**, respectively.

Table 8 Material-Vessel Stress, Strain and Porosity Quantities

Quantity, FISH	Description
$\{\sigma_{xx}, \sigma_{yy}, \sigma_{zz}, \sigma_{xy}, \sigma_{xz}, \sigma_{yz}\}$, `mv_ms{xx,yy,zz,xy,xz,yz}`	material stress (2D model: $\sigma_{zz} \equiv \sigma_{xz} \equiv \sigma_{yz} \equiv 0$)

[37] The deviator stress should not be confused with the deviatoric stress (Engelder, 1994). The amount by which the axial stress component departs from the confining pressure in a triaxial test is commonly called the differential stress in the rock mechanics and geological literature, and is used by Paterson and Wong (2005, p. 6) in the direct reporting of triaxial test results.

[38] The mean stress for the 2D model is defined as the average of the in-plane stresses. It is not obtained by setting $\sigma_{zz} \equiv 0$ in the expression for mean stress of the 3D model.

$\{\varepsilon_{xx},\varepsilon_{yy},\varepsilon_{zz},\varepsilon_{xy},\varepsilon_{xz},\varepsilon_{yz}\}$, **mv_me{xx,yy,zz,xy,xz,yz}**	material strain (2D model: $\varepsilon_{zz}\equiv\varepsilon_{xz}\equiv\varepsilon_{yz}\equiv 0$)
$\{\sigma_a,\sigma_r\}$, **mv_ms{a,r}**	axial & radial stress
$\{\varepsilon_a,\varepsilon_r\}$, **mv_me{a,r}**	axial & radial strain
σ_d, **mv_msd**	deviator stress
σ_m, **mv_msm**	mean stress
ε_d, **mv_med**	deviator strain
ε_v, **mv_mev**	volumetric strain
n, **mv_mn**	measurement-based porosity
n_w, **mv_wn**	wall-based porosity

The three measurement techniques measure the following quantities:

$$\begin{aligned} &\sigma_{ij}^m \quad \varepsilon_{ij}^m && \text{measurement-based (6 terms each, symmetric)} \\ &\sigma_k^w \quad \varepsilon_k^w && \text{wall-based (3 terms each)} \\ &\underbrace{\varepsilon_k^g}_{\substack{i,j=\{x,y,z\}\\ k=\{x,y,z,r\}}} && \text{guage-based (3 terms)} \end{aligned} \tag{13}$$

For the 2D model, the above equation satisfies the condition: $i,j,k=\{x,y\}$. The wall- and gauge-based techniques measure only the direct stress and strain components, which we denote by a single subscript (e.g., σ_{xx} is denoted by σ_x). The cylindrical and spherical cells measure the radial components (σ_r and ε_r).

The wall-based stress quantities are the average force on opposing walls divided by the corresponding cross-sectional area:

$$\sigma_k^w = \frac{\frac{1}{2}\left(\left(F_k^w\right)^- - \left(F_k^w\right)^+\right)}{A_k}, \quad k=\{x,y,z\} \quad \left(\text{2D model: } k=\{x,y\}\right) \tag{14}$$

where $\left(F_k^w\right)^-$ and $\left(F_k^w\right)^+$ are the total force on the walls in the negative and positive (k)-directions, respectively, and A_k is the specimen cross-sectional area perpendicular to direction-(k). For the cylindrical and spherical cells, the radial stress acting on the corresponding wall is

$$\sigma_r^w = \frac{-\sum F_r^w}{A_r} \quad \left(\text{cylindrical and spherical cells}\right) \tag{15}$$

where the numerator is the sum of the radial components of the forces on the wall, and A_r is the surface area of the wall. The surface areas are determined (by **mv_wAreaMode**, M_a) using either the current ($M_a = 0$) or initial ($M_a = 1$) vessel dimensions, and expressed in terms of the distances between opposing walls (d_k^w). For the polyaxial cell: $A_x = d_y^w d_z^w$, $A_y = d_x^w d_z^w$ and $A_z = d_x^w d_y^w$; for the cylindrical cell: $A_z = \pi\left(d_r^w\right)^2 \big/ 4$ and $A_r = \pi d_r^w d_z^w$; and for the spherical cell: $A_r = \pi\left(d_r^w\right)^2$. For the polyaxial cell of the 2D model: $A_x = d_y^w t\left(t=1\right)$ and $A_y = d_x^w t\left(t=1\right)$.

The wall-based strain quantities are based on the change of distance between opposing walls:

$$\varepsilon_k^w = \frac{d_k^w - \left(d_k^w\right)_o}{\left(d_k^w\right)_o}, \quad k = \{x, y, z, r\} \quad \left(\text{2D model: } k = \{x, y\}\right) \tag{16}$$

where d_k^w is the distance between opposing walls in direction-$\left(k\right)$, and $\left(d_k^w\right)_o$ is the initial distance between these walls. The gauge-based strain quantities are based on the change of distance between opposing gauge grains:

$$\varepsilon_k^g = \frac{d_k^g - \left(d_k^g\right)_o}{\left(d_k^g\right)_o}, \quad k = \{x, y, z, r\} \quad \left(\text{2D model: } k = \{x, y\}\right) \tag{17}$$

where d_k^g is the distance between opposing gauge grains in direction-$\left(k\right)$, and $\left(d_k^g\right)_o$ is the initial distance between these grains. The initial distances provide a reference for the strain measurement and can be reset by the FISH functions **mv_{w,g}StrainZero**.

5.2 Material Deformability

The deformability of a bonded material can be quantified by the effective isotropic elastic constants, and the deformability of a granular material can be quantified by the resilient modulus. The discussion begins by considering the stiffness tensor of PFC material. Then the definition and measurement of the effective isotropic elastic constants and resilient modulus are presented.

The stiffness tensor relates stresses to strains. The two fundamental assumptions of linear elastic theory are that (a) stress-strain relations are linear, and (b) deformations are reversible. The first

assumption is expressed by Hooke's law, giving 36 independent elastic constants. The existence of a unique strain-energy potential (from assumption b) reduces the number of independent elastic constants to 21. By assuming different levels of material symmetry, the number of independent elastic constants can be reduced significantly. For example, an *isotropic* system has the property that all directions are elastically equivalent and principal, which reduces the number of independent elastic constants to two. Therefore, a linear elastic isotropic material model has two independent elastic constants. A hexagonal system has a plane of elastic isotropy at each point, and these planes are parallel at all points. Such a body is said to be *transversely isotropic*, and there are five independent elastic constants. The stiffness tensor of the PFC material is affected by stress and damage so that, in general, the material response does not correspond with that of a linear elastic isotropic material model — e.g., the material response becomes transversely isotropic in response to both applied compression and compression-induced cracking (Potyondy and Hazzard, 2008).

The effective isotropic elastic constants are defined as the Young's modulus $\left(E\right)$ and Poisson's ratio $\left(\nu\right)$ of a linear elastic isotropic material model. It is useful to measure the effective isotropic elastic constants of the PFC material — e.g., when calibrating the bonded material, E and ν are compared with the elastic constants measured during triaxial tests on real rock specimens. The effective isotropic elastic constants are measured by performing a compression test on the PFC material and interpreting the macroscopic force-displacement response. The interpretation differs for the 3D and 2D models. The 3D model is an assembly of rigid three-dimensional grains for which stress and strain is defined in a straightforward fashion. The effective isotropic elastic constants of the 3D model are computed as

$$\begin{aligned} E &= \frac{\Delta\sigma_a}{\Delta\varepsilon_a} \\ \nu &= -\frac{\Delta\varepsilon_r}{\Delta\varepsilon_a} \end{aligned} \quad \left(\text{3D model}\right) \tag{18}$$

where the stress and strain components are defined in Section 5.1 such that σ_a is the axial stress, ε_a is the axial strain and ε_r is the radial strain measured during a compression test in which a constant confining pressure has been maintained during axial-strain application.

The 2D model is an assembly of rigid unit-thickness disks. The unit-thickness disks are rigid so that they do not expand in the out-of-plane direction and no stress acts in the out-of-plane direction; therefore, the out-of-plane stress and strain components are equal to zero. Note that this condition is neither plane strain nor plane stress. A material subjected to plane-strain conditions will be stiffer in its plane of loading than the same material subjected to plane-stress conditions, but plane-strain or plane-stress conditions cannot be imposed on the 2D model. The 2D model boundary conditions are

neither plane strain nor plane stress, because the corresponding stress-strain constitutive relations are not employed — i.e., the out-of-plane forces and displacements do not enter into the force-displacement law at the contact level.

In order to measure effective isotropic elastic constants of the 2D material, we perform a compression test on the material and *interpret* the macroscopic force-displacement response assuming either plane-strain or plane-stress conditions. For the same 2D model, one macroscopic force-displacement response is measured, but two sets of effective isotropic elastic constants, corresponding with plane-stress and plane-strain conditions, are computed as follows.

The plane-stress elastic constants are computed as

$$\begin{aligned} E' &= \frac{\Delta\sigma_a}{\Delta\varepsilon_a} \\ \nu' &= -\frac{\Delta\varepsilon_r}{\Delta\varepsilon_a} \end{aligned} \qquad \text{(2D model, plane stress)} \tag{19}$$

where the stress and strain components are defined in Section 5.1 such that σ_a is the axial stress, ε_a is the axial strain and ε_r is the radial strain (defined in Section 5.1) measured during a compression test in which a constant confining pressure has been maintained during axial-strain application. The above equation is valid for the case of plane stress $\left(\Delta\sigma_z = 0\right)$ and constant radial stress $\left(\Delta\sigma_r = 0\right)$ during the stress-strain increments. Then, the plane-strain elastic constants are obtained via

$$\begin{aligned} \nu &= \frac{\nu'}{1+\nu'} \\ E &= E'\left(1-\nu^2\right) \end{aligned} \qquad \text{(2D model, plane strain)} \tag{20}$$

which is the general relation between plane-stress and plane-strain conditions (Ugural and Fenster, 1987, p. 71).

How are the effective isotropic elastic constants of the 2D model used? When calibrating the 2D bonded material, E and ν (not E' and ν') are compared with the elastic constants measured during triaxial tests on real rock specimens. To what do the effective elastic constants correspond? If a region of a 2D isotropic elastic continuum were extracted and replaced with the 2D model material, and its corresponding set of elastic constants were assigned to the remaining continuum, then the deformation state of the model material would match that of the continuum — i.e., there would be full displacement compatibility along the extraction boundary. This procedure is used in the construction of 2D boundary-value models of excavation damage in which the model material is inserted into a pre-defined region within a larger continuum model. For a tunnel simulation, the

continuum model is run in plane-strain mode and assigned the plane-strain elastic constants E and ν.

The resilient modulus (M_R) is defined as the ratio of applied deviator stress to recoverable or "resilient" strain (see Figure 28). It is a granular material characterization parameter that is stress dependent. The resilient modulus is used to perform layered elastic analysis (LEA). LEA is utilized extensively for pavement system evaluation and is a means of calculating pavement response under loading. Each pavement layer is defined by its resilient modulus and Poisson's ratio, even though granular bases exhibit nonlinear elastoplastic behavior in laboratory and field applications. LEA is used because it is a relatively simple analysis procedure and, more importantly, pavement loading is generally of low enough magnitude that a linear-elastic approximation of pavement material behavior is deemed suitable (Potyondy et al., 2018). According to Han and Vanapalli (2016), the resilient modulus is "…the key soil property in the mechanistic pavement design methods to rationally characterize the resilient behavior of the pavement materials, analyze the fatigue failure of the surface layer, and dimension the multi-layer system of the pavement structure."

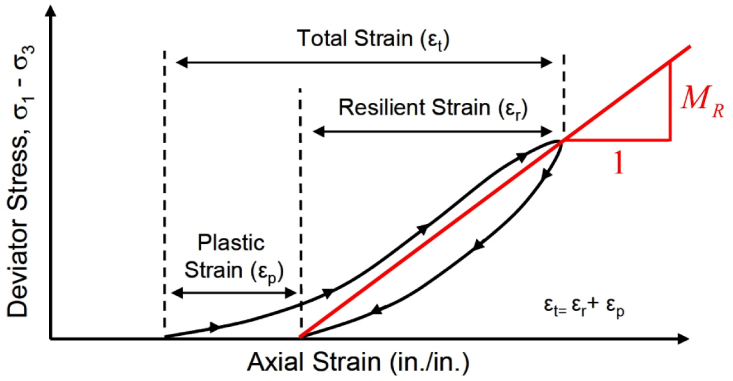

Figure 28 Response of granular material subjected to triaxial loading, and measurement of resilient modulus. (From Fig. 1 of Buchanan [2007].)

5.3 Servomechanism

The velocities of the walls of the polyaxial and cylindrical cells are controlled by a servomechanism. The servo-control procedure is described in Itasca (2008a&b, Section 3.10.5 Controlling Wall Velocity to Maintain Specified Stress, in *FISH* in *PFC3D*/*PFC2D* volumes). The servomechanism parameters are listed in Table 9. The polyaxial cell consists of three pairs of opposing walls for the 3D model and two pairs of opposing walls for the 2D model. The cylindrical cell consists of a pair of opposing axial walls and a cylinder wall. The spherical cell consists of a sphere wall. The boundary condition for each pair of walls as well as the cylinder and sphere walls can be either velocity or pressure. A velocity boundary condition sets the velocity of the wall pair to be equal and opposite and the velocity of the cylinder- and sphere-wall vertices to be radial (with a positive or negative value indicating opening or closing motion, respectively). A pressure boundary condition activates a

servomechanism that controls the velocities to maintain the specified pressure. The pressure acting on the opposing walls in the (k)-direction is given by

$$P_k^w = -\sigma_k^w, \quad \left(P_k^w > 0 \text{ is compression}\right)$$
$$\text{with } k = \begin{cases} \{x,y,z\}, & \text{polyaxial cell } \left(\text{2D model: } k = \{x,y\}\right) \\ \{z,r\}, & \text{cylindrical cell} \\ \{r\}, & \text{spherical cell.} \end{cases} \tag{21}$$

The servomechanism is turned on and off by **mvs_on** and **mvs_off**, respectively. When the servomechanism is on, the boundary conditions (set by **mvs_setBCs**) are enforced during subsequent cycling. Application of the specified pressures is determined by successful return from the **mvs_eqP** FISH function:

- **mvs_eqP(** ε_P **,** $n_{\lim}$ **)** cycles the model until either the pressures of all servo-controlled walls $\left(P_k^w\right)$ are within the equilibrium-pressure tolerance (ε_P) of the target values (P_k^t):

$$\left(\frac{\left|P_k^w - P_k^t\right|}{P_k^t} \le \varepsilon_P\right), \quad k = \{x,y,z,r\} \quad \left(\text{2D model: } k = \{x,y\}\right)$$

  or the number of steps (n_s) exceeds the step limit $\left(n_{\lim}\right)$:

$$n_s > n_{\lim} \quad \left[\text{command: solve max\_cycles } n_{\lim}\right].$$

Table 9 Servomechanism Parameters

Parameter	Type	Range	Def.	Description
$(B_c)_k$, **mvs_BC{x,y,z,r}**	INT	$\{0,1\}$	NA	boundary-condition code $\begin{cases} 0, \text{ velocity} \\ 1, \text{ pressure} \end{cases}, \quad k = \{x,y,z\} \text{ or } \{z,r\}$ (2D model: $k = \{x,y\}$)
$(B_v)_k$, **mvs_BC{x,y,z,r}Val**	FLT	$\{0,1\}$	NA	boundary-condition value $\begin{cases} v_k, \text{ velocity } \left((B_c)_k = 0\right) \\ P_k^t, \text{ pressure } \left((B_c)_k = 1\right) \end{cases}, \quad k = \{x,y,z\} \text{ or } \{z,r\}$ (2D model: $k = \{x,y\}$)
n_{gain},	FLT	$[1,\infty)$	25	servo gain update rate

mvs_gainUpdateRate				
$v_{\lim}$, **mvs_vLimit**	FLT	$(0.0,\infty)$	NA	velocity limit ($\lvert v_k \rvert \le v_{\lim}, v_{\lim} > 0$)

5.4 Loading Rate

The response of a real material and a DEM model are sensitive to loading rate. In most cases, we choose a loading rate that is slow enough to insure a quasi-static response. The quasi-static response is the response obtained when the test has been conducted under quasi-static conditions, which means that the loading has been slow enough that the system has time to adjust to the force redistribution that accompanies each nonlinear event (slip or bond breakage). This response could be obtained by performing a strain-controlled test, whereby the loading velocity is set to zero after each nonlinear event until the system reaches a new state of static equilibrium. In this way, we would trace out the stress-strain curve up to the peak, and the peak value would correspond with the quasi-static response. One can ensure that such a response has been obtained by conducting a strain-controlled test at a series of constant loading velocities, and demonstrating that the response is the same for all loading velocities below some critical velocity.

When calibrating a DEM model, we might compare the quasi-static response with the quasi-static response obtained for the real material (from a test that may have been performed at a different strain rate). This allows us to compare the results of the DEM model and the real material. If dynamic effects are also affecting the real system response, then these effects would also need to be included in the DEM model, which involves a more complex calibration process, whereby we match the dissipative mechanisms occurring in the real material. If we only compare quasi-static responses, then the dissipative mechanisms need not be replicated in the DEM model (e.g., the DEM model can be heavily damped by using local damping with a default damping coefficient of 0.7 to approximate quasi-static conditions).

The loading rate for the compression, diametral-compression, and direct-tension tests is the axial strain rate $(\dot{\varepsilon}_a)$. The axial strain rate should be chosen based on the previous considerations. Note that an axial strain rate that is sufficient to produce quasi-static loading on a specimen of a given length will most likely not produce quasi-static loading on a specimen of a different length. A reasonable estimate of the strain rate needed for the different-length specimen is found by equating the loading velocities for the two cases.

5.5 Compression Test

Compression tests (confined, unconfined and uniaxial strain) are performed upon specimens that are centered w.r.t. the origin. The specimens may have been created either in the physical material vessel or in the periodic material vessel and assembled into a block of material. If the specimen has been created in the physical material vessel, then the vessel walls are used to perform the test; otherwise,

the specimen is carved out of the block of material and walls are created. Carving is available only for 3D models. The walls provide a polyaxial or cylindrical cell. The polyaxial cell provides a polyaxial loading condition while the cylindrical cell provides a triaxial loading condition. The loading axis corresponds with the axial direction shown in Figure 20, and the loading conditions for the three test types are shown in Figure 27. The axial walls act as loading platens. For a confined test, the velocities of the radial walls are controlled by a servomechanism to maintain a constant confining pressure. For an unconfined test, the radial walls are moved away from the specimen and kept motionless.[39] For a uniaxial-strain test, the radial walls are kept motionless. The compression-test parameters are listed in Table 10. Compression testing is provided by the **`CompTest`** project, which is a subdirectory of the **`MatGen-X`** directory.

Table 10 Compression-Test Parameters

Parameter	Type	Range	Default	Description
Material-vessel parameters are listed in Table 6.				
B_c, **`sp_carve`**	INT	$\{0,1\}$	0	carve flag $\begin{cases} 0, \text{ do not carve} \\ 1, \text{ carve} \end{cases}$ If $B_c = 1$, then specify: shape, {H, W, D} and wall eff. modulus (see **`sp.p3fis`**).
T_t, **`ct_testType`**	INT	$\{0,1,2\}$	0	compression test type code $\begin{cases} 0, \text{ confined} \\ 1, \text{ unconfined} \\ 2, \text{ uniaxial strain} \end{cases}$
P_c, **`ct_Pc`**	FLT	$(0.0,\infty)$	NA	confining pressure ($P_c > 0$ is compression)
$\dot{\varepsilon}_a$, **`ct_eRate`**	FLT	$(0.0,\infty)$	NA	axial strain rate ($\lvert v \rvert = \frac{1}{2}\dot{\varepsilon}_a h_o$, $\dot{\varepsilon}_a > 0$, see Figure 27 and Section 5.4)
C_l, **`ct_loadCode`**	INT	$\{0,1\}$	0	loading-phase code $\begin{cases} 0, \text{ single stage} \\ 1, \text{ multiple stages} \end{cases}$
α, **`ct_loadFac`**	FLT	$(0.0,1.0)$	0.9	load-termination factor ($C_l = 0$) for

[39] The wall-based axial stress is computed using the axial cross-sectional area of the initial vessel. The wall-based radial stress, radial strain and volumetric strain are zero; the corresponding measurement-based quantities remain valid and are used by the hidden views **`pl-mer_wea`** and **`pl-mev_wea`**. The radial walls can be removed from model views by adding these walls to the filter of the wall plot item.

				termination criterion: $\left\|\sigma_d^w\right\| \le \alpha \left\|\sigma_d^w\right\|_{\max}$
Servo-control group:				
ε_P, **ct_PTol**	FLT	$(0.0,\infty)$	**pk_PTol**	pressure tolerance $\left(\frac{\left\|P-P_c\right\|}{P_c} \le \varepsilon_P\right)$ where P is current pressure
$\varepsilon_{\lim}$, **ct_ARatLimit**	FLT	$(0.0,\infty)$	1×10^{-5}	equilibrium-ratio limit (parameter of **ft_eq**)
$n_{\lim}$, **ct_stepLimit**	INT	$[1,\infty)$	**pk_stepLimit**	step limit (parameter of **ft_eq**)
$v_{\lim}$, **ct_vLimit**	FLT	$(0.0,\infty)$	$10H\dot{\varepsilon}_a$	servo velocity limit (see Table 9)

The compression test consists of a seating phase followed by a loading phase. During the seating phase, the strains are reset to zero. For a confined test, confining pressure is applied by activating the servomechanism with a pressure boundary condition in all directions. For an unconfined test, the radial walls are first moved away from the specimen, whereas for a uniaxial-strain test, the radial walls are kept in their initial position. Then for both unconfined and uniaxial-strain tests, an axial pressure (equal to P_c) is applied by activating the servomechanism with a pressure boundary condition in the axial direction and a velocity boundary condition of zero in the radial direction. Seating is successful if both **mvs_eqP()** and **ft_eq()** indicate that static-equilibrium has been obtained. The model state is saved at the end of the seating phase.

Grain displacements are reset to zero after the seating phase. At the start of the loading phase, strains are reset to zero. Then axial strain is applied by moving the axial walls at the specified strain rate while keeping the confining pressure constant for a confined test or keeping the radial walls motionless for either an unconfined or uniaxial-strain test. The loading phase may consist either of a single stage that ends when the applied deviator stress falls below a specified fraction of its peak value or multiple stages during which the axial-strain increments ($\Delta\varepsilon_a, \Delta\varepsilon_a > 0$ is opening) are specified in the function **ctPerformStages**. At the end of each stage, the axial wall velocities are set to zero and the model state is saved.

During the compression test, the crack-monitoring package is on (for bonded materials), and the specimen behavior is monitored using the history mechanism to sample and store relevant quantities. The monitored quantities include average stress and strain within the specimen and numbers of cracks (for bonded materials).

5.6 Diametral-Compression Test

Diametral-compression tests are performed upon specimens that are centered w.r.t. the origin. Axial walls that act as loading platens are created and centered w.r.t. the origin such that the loading axis

corresponds with the y-direction (see Figure 29). The platens are frictionless, and the grain-wall contact stiffness is set based on a specified effective modulus. The diametral-compression test parameters are listed in Table 11. Diametral-compression testing is provided by the **`DiamCompTest`** project, which is a subdirectory of the **`MatGen-X`** directory.

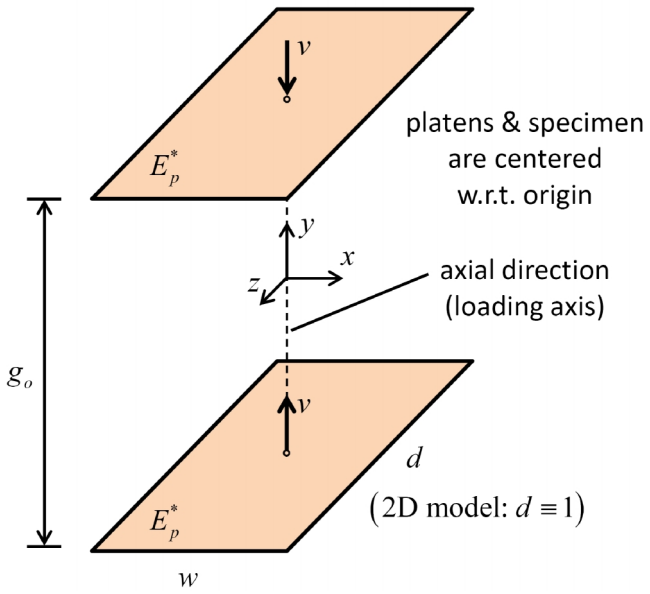

Figure 29 Loading configuration of diametral-compression test.

Table 11 Diametral-Compression Test Parameters

Parameter	Type	Range	Default	Description
$\{w,d\}$, **`dc_{w,d}`**	FLT	$(0.0,\infty)$	NA	platen width and depth (2D model: $d \equiv 1$)
g_o, **`dc_g0`**	FLT	$(0.0,\infty)$	NA	initial platen gap
E_p^*, **`dc_emod`**	FLT	$(0.0,\infty)$	**`mv_emod`** or NA	platen effective modulus (used by linear contact model)
$\dot{\varepsilon}_a$, **`dc_eRate`**	FLT	$(0.0,\infty)$	NA	axial strain rate ($\lvert v\rvert = \frac{1}{2}\dot{\varepsilon}_a g_o$, $\dot{\varepsilon}_a > 0$, see Figure 29 and Section 5.4)
C_l, **`dc_loadCode`**	INT	$\{0,1\}$	0	loading-phase code $\begin{cases} 0, \text{ single stage} \\ 1, \text{ multiple stages} \end{cases}$
α, **`dc_loadFac`**	FLT	$(0.0,1.0)$	0.9	load-termination factor ($C_l = 0$) for termination criterion: $\lvert F_a\rvert \le \alpha \lvert F_a\rvert_{\max}$
Static-equilibrium group:				

$\varepsilon_{\lim}$, **dc_ARatLimit**	FLT	$(0.0,\infty)$	1×10^{-5}	equilibrium-ratio limit (parameter of **ft_eq**)
α , **dc_stepLimit**	INT	$[1.0,\infty)$	**pk_stepLimit** or 2×10^{6}	step limit (parameter of **ft_eq**)

The diametral-compression test consists of a set-up phase followed by a loading phase. During the set-up phase, the walls are created and the system is brought to static equilibrium (via the **ft_eq** FISH function). The model state is saved at the end of the set-up phase.

Grain displacements are reset to zero after the set-up phase. During the loading phase, axial strain is applied by moving the axial walls at the specified strain rate ($\dot{\varepsilon}_a$). The loading phase may consist of either a single stage that ends when the axial-force magnitude falls below a specified fraction of its peak value, or multiple stages during which the axial-strain increments ($\Delta\varepsilon_a, \Delta\varepsilon_a > 0$ is opening) are specified in the function **dcPerformStages**. At the end of each stage, the wall velocities are set to zero and the model state is saved.

During the diametral-compression test, the crack-monitoring package is on, and the specimen behavior is monitored using the history mechanism to sample and store relevant quantities. The monitored quantities include axial force and axial strain. The axial force is the average force on the opposing walls:

$$F_a = \frac{1}{2}\left(\left(F_y\right)^- - \left(F_y\right)^+\right), \quad \left(F_a > 0 \text{ is tension}\right) \tag{22}$$

where $\left(F_y\right)^-$ and $\left(F_y\right)^+$ are the total force on the bottom and top walls, respectively. The axial strain is based on the change of distance between the opposing walls:

$$\varepsilon_a = \frac{g - g_o}{g_o}, \quad \left(\varepsilon_a > 0 \text{ is extension}\right) \tag{23}$$

where g is the wall gap, and g_o is the initial wall gap.

When the diametral-compression test is performed upon a cylindrical specimen oriented such that the loading axis coincides with the cylinder radial direction, then the Brazilian tensile strength is given by

$$\sigma_B = \frac{\left|F_a\right|_{\max}}{\pi R t}, \quad \left(\text{2D model: } t \equiv 1\right) \tag{24}$$

where $|F_a|_{\max}$ is the peak axial force, and R and t are the radius and thickness, respectively, of the Brazilian disk (Goodman, 1980).

5.7 Direct-Tension Test

Direct-tension tests are performed upon specimens that are centered w.r.t. the origin. The specimens may have been created either in the physical material vessel or in the periodic material vessel and assembled into a block of material, in which case they are carved out of the block of material. Carving is available only for 3D models. The loading axis corresponds with the axial direction shown in Figure 20. During the direct-tension test, the specimen is gripped at its ends and pulled apart slowly while monitoring the axial stress and strain (using the measurement-based quantities of σ_a^m and ε_a^m listed in Table 8). The direct-tension test parameters are listed in Table 12. Direct-tension testing is provided by the **`TenTest`** project, which is a subdirectory of the **`MatGen-X`** directory.

The specimen is gripped by identifying a thin layer of surface grains that will be used to load the specimen. The surface grains are referred to as grip grains and identified based on the specified grip thickness (t_g). The velocities of the grip grains are fixed in the axial direction, thereby pulling apart the opposing specimen surfaces. The grip grains are not allowed to translate or spin during the test, which is equivalent to the opposing surfaces being glued to flat and rigid platens. The velocity of the grip grains is specified via the axial strain rate ($\dot{\varepsilon}_a$).

Table 12 Direct-Tension Test Parameters

Parameter	Type	Range	Default	Description
Material-vessel parameters are listed in Table 6.				
B_c, **`sp_carve`**	INT	$\{0,1\}$	0	carve flag $\begin{cases} 0, & \text{do not carve} \\ 1, & \text{carve} \end{cases}$ If $B_c = 1$, then specify: shape and {H, W, D} (see **`sp.p3fis`**).
t_g, **`tt_tg`**	FLT	$(0.0,\infty)$	$0.1H$	grip thickness
$\dot{\varepsilon}_a$, **`tt_eRate`**	FLT	$(0.0,\infty)$	NA	axial strain rate ($\lvert v\rvert = \frac{1}{2}\dot{\varepsilon}_a h_o,\ \dot{\varepsilon}_a > 0$, see Figure 27 and Section 5.4)
C_l, **`tt_loadCode`**	INT	$\{0,1\}$	0	loading-phase code $\begin{cases} 0, & \text{single stage} \\ 1, & \text{multiple stages} \end{cases}$

α , **tt_loadFac**	FLT	$(0.0,1.0)$	0.9	load-termination factor ($C_l = 0$) for termination criterion: $\left\|\sigma_a^m\right\| \le \alpha \left\|\sigma_a^m\right\|_{\max}$

The direct-tension test consists of a set-up phase followed by a loading phase. During the set-up phase, the grip grains are identified (by assigning the names **ttGripTop** and **ttGripBottom** to the first slot of the group data for these grains), the motion of these grains is specified and the strains are reset to zero. The model state is saved at the end of the set-up phase.

Grain displacements are reset to zero after the set-up phase. During the loading phase, axial strain is applied by moving the grip grains at the specified strain rate. The loading phase may consist either of a single stage that ends when the axial stress falls below a specified fraction of its peak value or multiple stages during which the axial-strain increments ($\Delta\varepsilon_a, \Delta\varepsilon_a > 0$ is opening) are specified in the function **ttPerformStages**. At the end of each stage, the grip-grain velocities are set to zero and the model state is saved.

During the direct-tension test, the crack-monitoring package is on, and the specimen behavior is monitored using the history mechanism to sample and store relevant quantities. The monitored quantities include axial stress and axial strain within the specimen and numbers of cracks.

5.8 Fracture-Toughness Test

A fracture-toughness test is not provided in the material-modeling support package. It could be performed as illustrated in Figure 27, and described in Potyondy and Emam (2014a&b, Sections 16.0&12.0 Fracture Toughness (KIC) Measurement).

6.0 STRESS-INSTALLATION PROCEDURE

Stresses can be installed in the material that is formed in the periodic material vessel, and these stresses provide the initial stress state when the model is converted into a periodic brick and then assembled into a specimen for subsequent boundary-value modeling. The stress state has no shear components and does not vary with position. It would be relatively straightforward to enhance the procedure to support a general uniform stress state (with shear components) by following the procedure described in Itasca (2008a&b).[40] That procedure describes how to install a stress field that may vary linearly in space within an arbitrarily shaped particle ensemble. It has not been implemented in the current material-modeling support package.

[40] The description is in Section 3.9 Stress-Installation Procedure, in the *FISH in PFC3D/2D* volumes.

7.0 REFERENCES

Adair, R.K. (2002) ***The Physics of Baseball***, Third Edition, New York: HarperCollins.

Buchanan, S. (2007) "Resilient Modulus: What, Why, and How?" Vulcan Materials Company, August 31, 2007. [Document **`2-Resilient-Modulus-Buchanan.pdf`** accessed from www.vulcaninnovations.com/public/pdf on November 6, 2015.]

Cundall, P.A, and O.D.L. Strack. (1979) "A Discrete Numerical Model for Granular Assemblies," *Géotechnique*, ***29***, 47–65.

Engelder, T. (1994) "Deviatoric Stressitis: A Virus Infecting the Earth Science Community," *EOS Trans. AGU*, ***75***, 209.

Goodman, R.E. (1980) ***Introduction to Rock Mechanics***, New York: John Wiley & Sons.

Han, Z., and S.K. Vanapalli. (2016) "State-of-the-Art: Prediction of Resilient Modulus of Unsaturated Subgrade Soils," *Int. J. Geomechanics*, 10.1061/(ASCE)GM.1943-5622.0000631, 04015104.

Holt, R.M., J. Kjolaas, I. Larsen, L. Li, A. Gotusso Pillitteri and E.F. Sonstebo. (2005) "Comparison Between Controlled Laboratory Experiments and Discrete Particle Simulations of the Mechanical Behavior of Rock," *Int. J. Rock Mech. & Min. Sci., **42,*** 985–995.

Itasca Consulting Group, Inc. (2018) *PFC — Particle Flow Code in 2 and 3 Dimensions*, Version 6.0, Documentation Set of version 6.00.2. Minneapolis: Itasca.

Itasca Consulting Group, Inc. (2008a) *PFC3D — Particle Flow Code in 3 Dimensions*, Version 4.0, User's Manual. Minneapolis: Itasca.

Itasca Consulting Group, Inc. (2008b) *PFC2D — Particle Flow Code in 2 Dimensions*, Version 4.0, User's Manual. Minneapolis: Itasca.

McDowell, G.R., O. Harireche, M. Konietzky, S.F. Brown and N.H. Thom. (2006) "Discrete Element Modelling of Geogrid-Reinforced Aggregates," *Proceeding of the Institution of Civil Engineers — Geotechnical Engineering*, ***159***(1), 35–48.

Nicolson, C.R., A.M. Starfield, G.P. Kofinas and J.A. Kruse. (2002) "Ten Heuristics for Interdisciplinary Modeling Projects," *Ecosystems, **5***, 376–384.

Oreskes, N., K. Shrader-Frechette and K. Belitz. (1994) "Verification, Validation, and Confirmation of Numerical Models in the Earth Sciences," *Science, **263***, 641–646.

Paterson, M.S., and T.-f. Wong (2005) ***Experimental Rock Deformation — The Brittle Field***, Second Edition, Berlin: Springer-Verlag.

Potyondy, D.O. (2018) "A Flat-Jointed Bonded-Particle Model for Rock," paper ARMA 18-1208 in Proceedings of 52nd U.S. Rock Mechanics/Geomechanics Symposium, Seattle, USA, 17–20 June 2018.

Potyondy, D.O. (2017) "Simulating Perforation Damage with a Flat-Jointed Bonded-Particle Material," paper ARMA 17-223 in Proceedings of 51st U.S. Rock Mechanics/Geomechanics Symposium, San Francisco, USA, 25–28 June 2017.

Potyondy, D. (2019) "Hill Contact Model [version 4]," Itasca Consulting Group, Inc., Technical Memorandum ICG7795-L (April 5, 2019), Minneapolis, Minnesota.

Potyondy, D. O. (2015) "The Bonded-Particle Model as a Tool for Rock Mechanics Research and Application: Current Trends and Future Directions," *Geosystem Engineering,* ***18***(1), 1–28.

Potyondy, D.O., and P.A. Cundall. (2004) "A Bonded-Particle Model for Rock," *Int. J. Rock Mech. & Min. Sci.*, ***41***(8), 1329–1364.

Potyondy, D., and S. Emam. (2014a) "*PFC3D* 4.0 Manual Modifications," Itasca Consulting Group, Inc., Technical Memorandum distributed with *PFC3D* 4.0 executable (February 6, 2014), Minneapolis, Minnesota.

Potyondy, D., and S. Emam. (2014b) "*PFC2D* 4.0 Manual Modifications," Itasca Consulting Group, Inc., Technical Memorandum distributed with *PFC2D* 4.0 executable (February 6, 2014), Minneapolis, Minnesota.

Potyondy, D.O., and J.F. Hazzard. (2008) "Effects of Stress and Induced Cracking on the Static and Dynamic Moduli of Rock," in ***Continuum and Distinct Element Numerical Modeling in Geo-Engineering 2008*** (Proc. 1st Int. FLAC/DEM Symposium, Minneapolis, Minnesota, USA, August 25–27, 2008), pp. 147–156, R. Hart, C. Detournay and P. Cundall, Eds., Minneapolis, MN: Itasca Consulting Group.

Potyondy, D., J. Siekmeier, and L. Petersen. (2016) "Aggregate-Geogrid Interaction Model Incorporating Moisture Effects," in Transportation Research Board 2016 Annual Meeting Compendium of Papers.

Santamarina, J.C., K.A. Klein and M.A. Fam. (2001) ***Soils and Waves: Particulate Materials Behavior, Characterization and Process Monitoring***, New York: John Wiley & Sons, Ltd.

Siekmeier, J., J. Bittmann, D. Potyondy, and L. Petersen. (2016) "Introducing a Geogrid Gain Factor for Flexible Pavement Design," in *Proceedings University of Minnesota 64th Annual Geotechnical Engineering Conference* (Saint Paul, MN, March 4, 2016).

Starfield, A.M. (1997) "A Pragmatic Approach to Modeling for Wildlife Management," *J. Wildlife Management,* ***61***(2), 261–270.

Starfield, A.M., and P.A. Cundall. (1988) "Towards a Methodology for Rock Mechanics Modelling," *Int. J. Rock Mech. Min. Sci. & Geomech. Abstr.,* ***25***(3), 99–106.

Ugural, A.C., and S.K. Fenster. (1987) ***Advanced Strength and Applied Elasticity***, Second SI Edition, New York: Elsevier Science Publishing Co., Inc.

Winsberg, E. (2010) ***Science in the Age of Computer Simulation***, Chicago: University of Chicago Press.